Quantifying stratospheric ozone trends over 1984-2020: A comparison of ordinary and regularized multivariate regression models

Yajuan Li[1,2], Sandip S. Dhomse[3,4], Martyn P. Chipperfield[3,4], Wuhu Feng[3,5], Jianchun Bian[2,6,7], Yuan Xia[1] and Dong Guo[8]
1 School of Electronic Engineering, Nanjing Xiaozhuang University, Nanjing, China
2 Key Laboratory of Middle Atmosphere and Global Environment Observation, Institute of Atmospheric Physics, Chinese Academy of Sciences, Beijing, China
3 School of Earth and Environment, University of Leeds, Leeds, UK
4 National Centre for Earth Observation (NCEO), University of Leeds, Leeds, UK
5 National Centre for Atmospheric Science (NCAS), University of Leeds, Leeds, UK
6 College of Earth and Planetary Sciences, University of Chinese Academy of Sciences, Beijing, China
7 College of Atmospheric Sciences, Lanzhou University, Lanzhou, China
8 Key Laboratory of Meteorological Disaster, Ministry of Education/Joint International Research Laboratory of Climate and Environment Change/Collaborative Innovation Center on Forecast and Evaluation of Meteorological Disasters, Nanjing University of Information Science & Technology, Nanjing, China

Correspondence to: Yajuan Li (yajuanli@njxzc.edu.cn) and Sandip S. Dhomse (s.s.dhomse@leeds.ac.uk)

Abstract. Accurate quantification of long-term trends in stratospheric ozone can be challenging due to their sensitivity to natural variability, the quality of the observational datasets, non-linear changes in forcing processes as well as the statistical methodologies. Multivariate linear regression (MLR) is the most commonly used tool for ozone trend analysis, however, the complex coupling in many atmospheric processes can make it prone to the issue of over-fitting when using the conventional Ordinary Least Squares (OLS) approach. To overcome this issue, here we adopt a regularised (Ridge) regression method to estimate ozone trends and quantify the influence of individual processes. We use the Stratospheric Water and OzOne Satellite Homogenized (SWOOSH) merged data set (v2.7) to derive stratospheric ozone profile trends for the period 1984-2020. Beside SWOOSH, we also analyse a machine-learning-based satellite-corrected gap-free global stratospheric ozone profile dataset from a chemical transport model (ML-TOMCAT), and output from a chemical transport model (TOMCAT) simulation forced with ECMWF ERA5 reanalysis.

For 1984-1997, we observe smaller negative trends in the SWOOSH stratospheric ozone profile using Ridge regression compared to OLS. Except for the tropical lower stratosphere, the largest differences arise in the mid-latitude lowermost stratosphere (>4% per decade difference at 100 hPa). Since 1998, and the onset of ozone recovery in the upper stratosphere, the positive trends estimated using the Ridge regression model (~1% per decade near 2 hPa) are smaller than those in OLS (~2% per decade). In the lower stratosphere, post-1998 negative trends with large uncertainties are observed and Ridge-based trend estimates are somewhat smaller and less variable in magnitude compared to the OLS regression. Aside from the tropical lower stratosphere, the largest difference is around 2% per decade at 100 hPa (with ~3% per decade uncertainties for individual trends) in northern midlatitudes. For both time periods the SWOOSH data produces large negative trends in the tropical lower stratosphere with a correspondingly large difference between the two trend methods. In both cases the Ridge method produces a smaller trend. The regression coefficients from both OLS and Ridge models, which represent ozone variations associated with natural processes (e.g., the quasi-biennial oscillation, solar variability, El Niño-Southern Oscillation, Arctic oscillation, Antarctic oscillation, and Eliassen-Palm flux), highlight the dominance of dynamical processes in controlling lower stratospheric ozone concentrations. Ridge regression generally yields smaller regression coefficients due to correlated explanatory variables, and care must be exercised when comparing fit coefficients and their statistical significance across different regression methods.

Comparing the ML-TOMCAT-based trend estimates with the ERA5-forced model simulation, we find ML-TOMCAT shows significant improvements with much better consistency with the SWOOSH data set, despite the ML-TOMCAT training period overlapping with SWOOSH only for the Microwave Limb Sounder (MLS) measurement period. The largest

inconsistencies with respect to SWOOSH-based trends post-1998 appear in the lower stratosphere where the ERA5-forced model simulation shows positive trends for both the tropics and mid-latitudes. The large differences between satellite-based data and the ERA5-forced model simulation confirm significant uncertainties in ozone trend estimates, especially in the lower stratosphere, underscoring the need for caution when interpreting results obtained with different regression methods and data sets.

1 Introduction

With the success of the Montreal Protocol and its amendments, the emission of major ozone-depleting substances (ODSs) has greatly reduced and observations show decreases in their atmospheric concentrations (e.g. Anderson et al., 2000; Solomon et al., 2006; Chipperfield et al., 2017; Montzka et al., 2021). However, quasi-global total column ozone does not show a statistically significant ozone increase (WMO, 2022 and references therein). To some certain extent, there is a scientific consensus that the ODS-related positive ozone trends are balanced by the negative contributions from atmospheric dynamics (e.g., Weber et al., 2022; Bognar et al., 2022). As the impacts of chemical and dynamical processes on ozone variability are variable across the stratosphere, accurate quantification of stratospheric ozone trends remains an unresolved challenge.

An important aspect of long-term ozone trends that has been confirmed by various recent studies is that there is an ozone increase in the upper stratosphere (e.g. Harris et al., 2015; Chipperfield et al., 2017; Sofieva et al., 2017; Ball et al., 2017; Steinbrecht et al., 2017; Petropavlovskikh et al., 2019; Godin-Beekmann et al., 2022), partly due to the decreased ODS concentrations and partly due to the stratospheric cooling resulting from increased greenhouse gases (GHGs). However, our understanding about the evolution of lower stratospheric ozone remains highly uncertain. Various observation-based studies suggest that there has been a continued decline in lower stratospheric ozone since 1998, both in the tropics and mid-latitudes (e.g. Ball et al., 2018; 2019a; Wargan et al., 2018; Orbe et al., 2020; Bognar et al., 2022), while model simulations do not reproduce these trends (Ball et al., 2020; Dietmüller et al., 2021; Davis et al., 2022; Li et al., 2022). It is well established that ozone in the lower stratosphere is sufficiently long-lived and primarily controlled by transport and circulation changes (e.g. Chipperfield et al., 2018). The increasing GHGs induce a strengthening of tropical upwelling and enhance the stratospheric circulation, which causes tropical ozone to decline in the lower stratosphere (Marsh et al., 2016). Besides, the non-linear quasi-biennial oscillation (QBO) and the El Niño–Southern Oscillation (ENSO) influence the dynamical variability in the lower stratosphere and drive the large interannual ozone variability in this region (Ball et al., 2019a; Diallo et al., 2018). The asymmetrical change pattern in the Brewer-Dobson circulation (BDC), with a relative slowdown in the northern hemisphere (NH), also provides evidence pointing to dynamically driven ozone variability in the lower stratosphere (e.g. Mahieu et al., 2014; Stiller et al., 2017; Prignon et al., 2021; Bognar et al., 2022). Considering the inconsistencies between observations and model simulations, it is important to gain better insight about the causes of uncertainties in the estimates of the lower stratospheric ozone trends.

Most importantly, the quantification of stratospheric ozone trends is not only sensitive to the natural variability and non-linear forcing processes, it also depends on the quality of the observational datasets and the time periods considered. To determine the long-term ozone trends and the attribution of ozone variability, composites of observations are generally used by merging different ozone observational data sets into a long, multi-decadal record. However, there are artefacts in the uncertainty budget and sampling inconsistencies between various datasets. Previous studies have used multiple composites merged from different observing platforms and discussed the sensitivity of ozone trends to the inclusion of new datasets (Ball et al., 2018, 2019; Sofieva et al., 2017, 2022; Steinbrecht et al., 2017; Petropavlovskikh et al., 2019; Weber et al., 2022; Godin-Beekmann et al., 2022). Here, we use the merged Stratospheric Water and OzOne Satellite Homogenized (SWOOSH, version 2.7) data set to assess the stratospheric ozone trends (Davis et al., 2016) for the 1984-2020 time period. In addition, a machine-learning-based satellite-corrected gap-free global stratospheric ozone profile dataset from a chemical transport model (ML-TOMCAT, Dhomse et al., 2021) is also used for comparison.

To improve the assessment of the long-term ozone trends and variability, multivariate linear regression (MLR) models with different configurations are most widely used by separating the influence of various chemical and dynamical processes on the ozone concentrations (e.g. Dhomse et al., 2006, 2022; Chehade et al., 2014; Li et al., 2020, 2022). Szeląg et al. (2020) analyzed the seasonal dependence of stratospheric ozone trends from four merged satellite datasets over 2000–2018 using a two-step MLR approach. Godin-Beekmann et al. (2022) presented the evaluation of stratospheric ozone profile trends in the extra-polar region over the period 2000–2020 with an updated version of the Long-term Ozone Trends and Uncertainties in the Stratosphere (LOTUS) regression model which additionally included seasonal trend terms. Bognar et al. (2022) used both MLR and dynamical linear modelling (DLM) methods (Laine et al, 2014; Ball et al., 2017, 2019a) to determine the stratospheric ozone trends during 2000–2021 with a combination of three satellite datasets. Recently, Dhomse et al. (2022) used an ensemble of MLR models and regularised regression methods (Ridge, Lasso and ElasticNet) to estimate the solar cycle signal in the observed and simulated ozone profiles for 2005-2020. With the extended datasets and improved statistical methodologies, there is better agreement and reduced uncertainties in different satellite-based ozone trends. However, it should be noted that trends in the lower stratosphere are still masked by large dynamical/natural variability.

Additional complications also arise from the use of chemical/dynamical proxies in the MLR; some of them are inevitably correlated and coupled, causing an issue of over-fitting (e.g. Dhomse et al., 2022), which will significantly lead to inconsistent and unreliable parameter estimates in regression modelling (e.g. Shariff and Duzan, 2018). To overcome this over-fitting problem, regularised regression models such as Ridge regression are highly recommended (e.g. Hoerl and Kennard, 1970). Previous studies have indicated that Ridge regression performs better than other estimators and can produce reliable results when explanatory variables are correlated (e.g. Shariff and Duzan, 2018; Tirink et al., 2020; Gana, 2022). In this paper, we use MLR models based on both OLS and Ridge regression methods to compare and discuss their differences in estimating stratospheric ozone trends. Besides SWOOSH and ML-TOMCAT data sets, a chemical transport model (TOMCAT) simulation forced with the European Centre for Medium-Range Weather Forecasts (ECMWF) ERA5 reanalyses (Li et al., 2022) is also used for comparison with satellite-based ozone trends and ozone changes associated with natural variability.

The paper is organized as follows. Section 2 describes the merged satellite-based ozone data set (SWOOSH), a TOMCAT model simulation forced with ECMWF ERA5 reanalyses (hereafter ERA5), and a machine-learning-based satellite-corrected TOMCAT product (ML-TOMCAT). Section 3 describes the MLR models and regression methods based on OLS and Ridge. Section 4 presents results regarding the ozone profile trends based on OLS and Ridge regression methods and the ozone variations associated with natural processes. Our conclusions are summarized in Section 5.

2 Data

2.1 SWOOSH

The Stratospheric Water and OzOne Satellite Homogenized (SWOOSH) data set is a monthly mean record of stratospheric ozone and water vapour data from a subset of limb sounding and solar occultation satellites operating from 1984 to present (Davis et al., 2016). It is obtained from https://csl.noaa.gov/groups/csl8/swoosh/ (last access: Jan 2023). The SWOOSH (v2.7) record is comprised of several individual satellite data from the Stratospheric Aerosol and Gas Experiment (SAGE-II/III v7/v4), the Upper Atmospheric Research Satellite Halogen Occultation Experiment (UARS HALOE v19), the UARS Microwave Limb Sounder (MLS v5/6), the Aura MLS (v5), the Aura High Resolution Dynamics Limb Sounder (HIRDLS v7) and the Atmospheric Chemistry Experiment - Fourier Transform Spectrometer (ACE-FTS v3.6) instruments, as well as a combined data product. The corrections that vary with latitude and height are determined from coincident observations closely matched in space and time during time periods of instrument overlap. The primary SWOOSH product consists of zonal-mean values at grids of 2.5, 5 and 10° resolution. There are filled and unfilled versions of the data set on both geographical and equivalent latitude coordinates. Many previous studies have demonstrated the reliability of this product in analyzing the variability and mechanisms associated with stratospheric ozone (e.g. Lu et al., 2019; Shangguan et al., 2019; Zhang et al., 2021; Hu et al., 2022). Here we use the gap-filled SWOOSH data at grids of 2.5° and 12 levels per decade ranging from 316 to 1 hPa (31 pressure levels). This SWOOSH data is considered a beta product and will continue to be updated as long as new data are available from the Aura MLS instrument or a suitable replacement.

2.2 TOMCAT simulation

Chemical transport models (CTMs) are important tools for understanding past ozone changes by combining up-to-date knowledge about various physical and chemical processes within a mathematically consistent framework. TOMCAT/SLIMCAT (hereafter TOMCAT) is a global 3-D off-line CTM (Chipperfield, 2006), which contains a detailed description of stratospheric chemistry (e.g. Feng et al., 2011, 2021; Dhomse et al., 2015, 2016; Chipperfield et al., 2018) or tropospheric chemistry (Monks et al., 2017) and uses winds and temperatures from meteorological analyses (usually ECMWF) to specify the atmospheric transport and temperatures.

Here we have performed a TOMCAT simulation (ERA5), which is forced with ECMWF ERA5 (Hersbach et al., 2020) reanalysis (e.g. Dhomse et al., 2019; Feng et al., 2021; Li et al., 2022). The ERA5 reanalysis has been released by ECMWF to supersede ERA-Interim which covered January 1979 to August 2019, with more and newer observations assimilated in ERA5. The inhomogeneities in reanalysis data sets could introduce spurious transport features (e.g. Schoeberl et al., 2003; Ploeger et al., 2015), and thus cause inability of chemical models to simulate the observed stratospheric ozone changes (Li et al., 2022). The TOMCAT simulation is identical to that used in Li et al. (2022), with 2.8° × 2.8° (T42 Gaussian grid) horizontal resolution and 32 hybrid sigma-pressure levels ranging from the surface to about 60 km. The 6-hourly grid point meteorological fields are interpolated linearly in time for the simulation.

2.3 ML-TOMCAT

We use a machine-learning-based method and chemically self-consistent output from the TOMCAT 3-D CTM to create a satellite-corrected long-term stratospheric ozone profile data set (ML-TOMCAT, Dhomse et al., 2021a). The TOMCAT setup is described in Sect. 2.2 above. A random-forest (RF) regression model, including five terms: passive ozone (O_3), HCl mixing ratio (HCl), methane mixing ratio (CH_4), Mg II solar flux term (MgII) as well as observation–model total column ozone difference (dTCO), is applied to the observation–model ozone difference by selecting 20 years of UARS-MLS (1991–1998) and AURA-MLS (2005–2016) measurements as a training period. The passive O_3, HCl and CH_4 are tracers taken from TOMCAT output fields, dTCO is calculated from Copernicus Climate Change Service (C3S) total ozone data, and the MgII index (Snow et al., 2014) is obtained from http://www.iup.uni-bremen.de/UVSAT/ Datasets/mgii (last access: Jan 2023). These variables account for possible biases in CTM profiles due to transport, solar flux variability or the use of coarse spectral bins (e.g. Dhomse et al., 2013; Sukhodolov et al., 2016; Feng et al., 2021).

The results show that ML-TOMCAT ozone concentrations are in excellent agreement with SWOOSH data and they are well within uncertainties of the observational data sets at almost all stratospheric levels. ML-TOMCAT is also ideally suited for the evaluation of chemical model ozone profiles and observation-based data sets from the tropopause up to 0.1 hPa. The ML-TOMCAT ozone profile data (v1.0) on pressure and altitude levels in mixing ratios and number density units are available via https://doi.org/10.5281/zenodo.5651194 (Dhomse et al., 2021b).

3 Methods

3.1 Multivariate linear regression models

Here we use multivariate linear regression (MLR) models to estimate the stratospheric ozone trends and to separate the influence of important chemical and dynamical processes on the ozone variations. The MLR setup is a modified version from that used in Dhomse et al. (2022). Briefly, it has 77 terms, including 24 monthly linear trend terms and 24 intercept terms for the independent linear trends (ILT, e.g. Weber et al., 2018) before and after the turnaround year (1997) close to the timing of the peak stratospheric halogen loading, 24 QBO terms at 30 and 50 hPa, and 5 proxies for the 11-year solar cycle, El-Nino Southern Oscillation (ENSO), Arctic Oscillation (AO), Antarctic Oscillation (AAO) and Eliassen-Palm (EP) flux. QBO, ENSO, AO and AAO indices are from Climate Prediction Center (https://www.cpc.ncep.noaa.gov/, last access: Jan 2023). The proxy for EP flux uses the 50 hPa vertical component (Fz50) with 2-month mean values (averaged over previous and current months) integrated over mid-latitudes between 45° and 75° in each hemisphere from the ECMWF ERA5 reanalysis. The effects of the aerosol loading from volcanic eruptions (e.g. Mt. Pinatubo 1991) are not considered in the MLR as we remove the data from 1991 to 1994. Here, we use twelve (monthly) trend terms instead of one (annual) as it is better at capturing seasonal patterns, and has better sensitivity to short-term fluctuations and improved flexibility that means better goodness of fit (R^2). And more proxies are considered to account for the dynamical variability of stratospheric ozone and to separate the influence of individual processes (e.g. Dhomse et al., 2022; Weber et al., 2022).

We apply the MLR to monthly mean ozone anomalies and get

$$\mathrm{d}O_3(t) = \sum_{j=1}^{77} \beta_j \times P_j(t) + \epsilon(t)$$

where $dO_3(t)$ denotes monthly mean ozone anomaly time series from 1984-2020 obtained by referencing the monthly mean $O_3(t)$ to the climatological mean for each calendar month. The explanatory proxies P_j include 77 terms which are de-trended (except for the linear trend terms) and normalised between 0 and 1. The coefficients β_j are obtained by least squares fitting of the residuals. By de-trending, the long-term trends in various proxies are moved to the linear trend terms, that is, the independent linear trends in the MLR combine both the dynamic and the ODS-related chemical trends (Weber et al., 2022).

As noted earlier, as most atmospheric processes are not completely independent, the MLR models suffer from over-fitting issues to a certain extent. Here we use both ordinary least squares (OLS) and regularised (Ridge) linear regression models for comparison to quantify the estimated ozone trends and the influence of individual processes.

3.2 OLS regression

Ordinary least squares (OLS) regression is a common method used to study the relationship between explanatory variables and response variables in regression models. The OLS method aims to minimize the sum of squared errors (SSE) between the observed values (y_i) and predicted values ($\widehat{y}_i$). The cost function being minimized is written as

$$\text{minimize } (\text{SSE} = \sum_{i=1}^{n} (y_i - \widehat{y}_i)^2)$$

It should be noted that the OLS with unbiased estimators performs well only when all key regression assumptions are satisfied, e.g. linear relationship, more observations (n) than features (p), no or little collinearity among the explanatory variables. Additionally, the OLS model is designed to minimise the residual errors but with relatively high variance, which means small changes in explanatory variables can lead to large changes in the estimated regression coefficients. Thus, care is needed when analysing the results of parameter estimates and inference under the OLS procedure.

3.3 Ridge regression

To overcome the over-fitting issue in regression, several methods have been developed and the most common is Ridge regression (Hoerl and Kennard, 1970). Ridge regression is a type of regularized regression which adds a penalty (called an L2 penalty) as described in Hastie et al. (2009) and Kuhn and Johnson (2013) to constrain the magnitudes and fluctuations of the coefficient estimates. This constraint helps to reduce the variance of the model at the expense of no longer being unbiased, which is a reasonable compromise. The cost function with a penalty term is written as

$$\text{minimize } (\text{SSE} + \alpha \sum_{j=1}^{p} {\beta_j}^2)$$

The penalty is calculated as the square of the magnitude of coefficients. By adding this penalty term, all coefficients of the regression variables (β_j) will be constrained or shrunk, but not to zero, so they all remain in the model. The strength of the penalty term is controlled by a tuning parameter (α). When this tuning parameter is set to zero, Ridge regression equals OLS regression. If $\alpha = \infty$, all coefficients in the regression are shrunk to zero. The ideal penalty is therefore somewhere in between 0 and ∞ that helps to control the model from over-fitting or under-fitting. Here we use cross-validation (CV) to identify the optimal α value (Pedregosa et al., 2011). The Ridge regression model used here is from the Python scikit module (for details see https://scikit-learn.org/stable/modules/ linear_model.html, last access: Jan 2023).

Figure 1 shows the SWOOSH ozone anomalies and fitting from OLS and Ridge regression models near the Equator (~1°N) at pressure levels of 1, 10 and 46.4 hPa. The cross-validated MSE (the average of all the test MSEs calculated from different training and testing sets) and coefficients for the Ridge regression model are also shown as the α value grows from 0.01 to 100. In all cases shown in **Figure 1**, we find a slight improvement in the MSE as the penalty (α) gets larger, suggesting that a regular OLS model likely over-fits the training data. As the penalty continues to increase, coefficients in the Ridge regression model are shrunk until close to zero. The vertical dashed lines represent the optimal α value with the minimum MSE ($\alpha_0 = 0.174$, 0.048 and 0.026 in Ridge regression for ozone anomaly data at pressure levels of 1, 10 and 46.4 hPa). Monthly mean ozone anomalies as well as the OLS and Ridge fitting from ML-TOMCAT and simulation ERA5 are shown in the supplement (**Figures S1-2**).

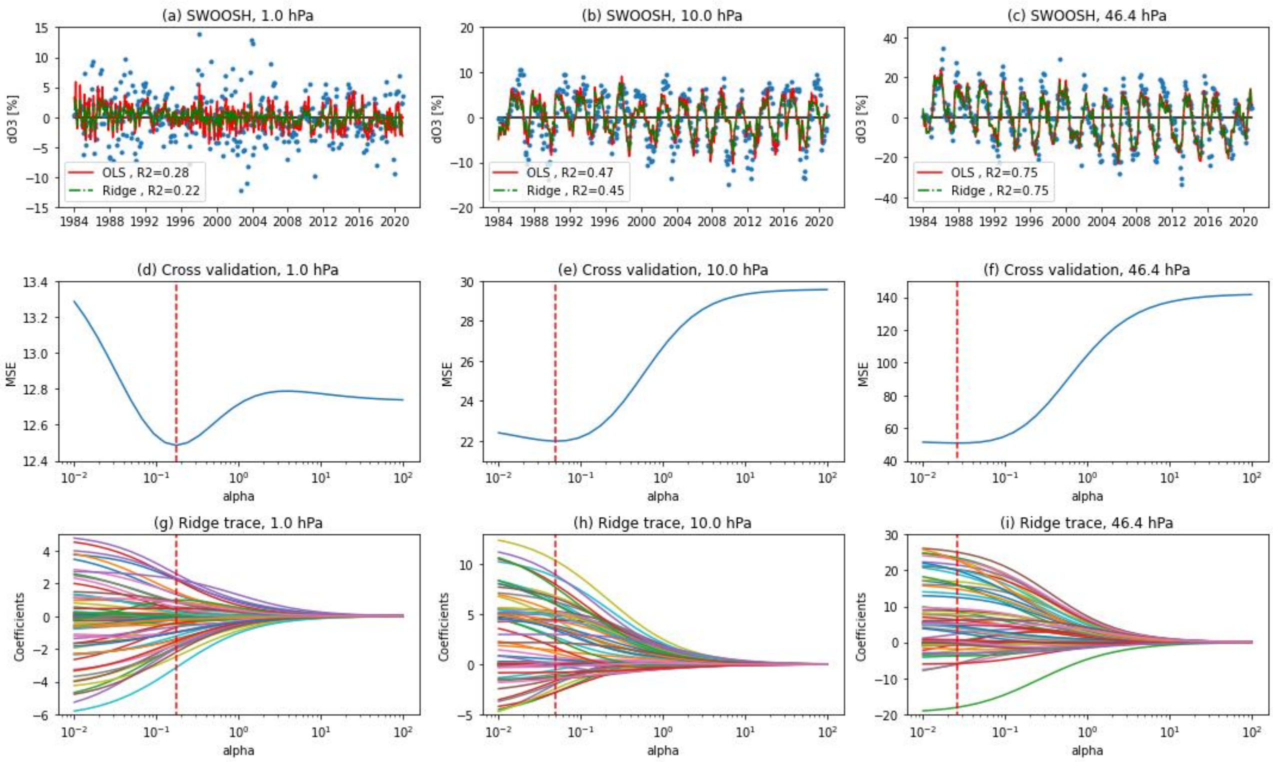

Figure 1: (a-c) Monthly mean ozone anomalies (blue dots) and the OLS (red line) and Ridge fitting (green dot-dashed line) from SWOOSH data during 1984-2020 at the pressure levels of 1 hPa (left column), 10 hPa (middle column) and 46.4 hPa (right column) for the 1°N latitude. (d-f) Cross-validated MSE values as well as (g-i) Ridge regression trace of the coefficients that change with alpha (α) are also shown. The vertical red dashed line indicates the optimal tuning value (α_0) for Ridge regression where MSE is minimum.

As expected, goodness of fit (R^2) values for Ridge regression are smaller than OLS whenever the ozone data is noisy and the regression model is not able to attribute ozone variations to any explanatory variables (e.g. upper stratosphere). However, R^2 differences are smaller when one or multiple variables are able to explain ozone variations (e.g. lower stratosphere). We use the Cochrane-Orcutt method to correct for the first-order autocorrelation (AR1) in the residuals of an OLS regression model. The procedure is performed iteratively with the covariance matrix updated for each iteration until the autocorrelation coefficient has converged sufficiently (Cochrane-Orcutt, 1949; Prais and Winsten, 1954). This correction for AR1 in the OLS regression model is widely used for the trends from monthly mean ozone time series (e.g. Dhomse et al., 2006; Ball et al., 2019; Petropavlovskikh et al., 2019; Bognar et al., 2022; Godin-Beekmann et al., 2022). However, Ridge regression, which constrains the fit coefficients by introducing a penalty term, is different from the linear unbiased estimates of the usual least squares method. If we still apply the AR1 correction to Ridge regression similar to OLS regression, the estimated regression coefficients can be affected; the correlation between the regression model and underlying data becomes very poor after "correction", and the regression in this case is under an "under-fitting" state with a very large tuning parameter. Besides, the autocorrelation coefficient does not always converge during iteration which makes it impossible to obtain the covariance matrix as in OLS regression. Given all this we do not apply the AR1 correction to Ridge regression here, and care must be taken of the limitations and assumptions of the Cochrane-Orcutt method.

4 Results and Discussion

4.1 Ozone profile trends with OLS and Ridge regression

Figure 2 shows the annual mean stratospheric ozone profile trends (% per decade) compared between OLS and Ridge regression methods for three latitude bands (60-35°S, 20°S-20°N and 35-60°N) from SWOOSH, ML-TOMCAT and the model simulation ERA5 over the period 1984-1997. The trend results as well as the 2σ uncertainties (the standard deviation of the trends) for several pressure levels (1, 2, 10, 46.4 and 100 hPa) are given in **Table 1**. The annual mean trend is the average of the twelve-monthly means, and the uncertainty of the annual trend is the standard deviation from taking the mean from the monthly values.

With Ridge regression, the stratospheric ozone profile trends from SWOOSH data show smaller declines during 1984-1997 compared to OLS-based trend estimates. As shown in **Figure 2 (a-c)** and **Table 1**, large OLS-Ridge differences appear in the upper stratosphere (~1 % per decade at 2 hPa) and the lowermost stratosphere (>4 % per decade at 100 hPa). Compared with the trend profiles derived from OLS regression, the Ridge regression model has less variability and smaller absolute fit coefficients (especially at mid-latitudes). These differences in trend values are likely due to the fundamental differences between the two regression methods. The largest ozone decreases appear in the tropical lower stratosphere (with about -30 % per decade for OLS and -12 % per decade for Ridge regression) although there are large uncertainties (>20 % per decade). These large uncertainties to some extent are associated with the considerable dynamical variability near the tropopause (e.g. Sofieva et al., 2014; Thompson et al., 2021; Bognar et al., 2022), and also are related to the quality of the satellite data and limitations in sampling and resolution (Davis et al., 2016). The negative ozone trend estimates from ML-TOMCAT and simulation ERA5 show very good agreement with those from SWOOSH data at mid-latitudes in both the Northern Hemisphere (NH) and Southern Hemisphere (SH). Large differences appear in the tropical middle and lower stratosphere where ML-TOMCAT and the ERA5-forced model simulation show positive trends with a range of 2-4 % per decade near 30 hPa but SWOOSH data show a near-zero trend. We note that there are large uncertainties in the lower stratosphere for both satellite data and model simulations.

Table 1: Stratospheric ozone trends with 2σ uncertainties (in % per decade) from SWOOSH during 1984-1997 based on OLS and Ridge regression.

Levels (hPa)	60-35°S		20°S-20°N		35-60°N	
	OLS	Ridge	OLS	Ridge	OLS	Ridge
1	-3.2 (2.6)	-1.8 (2.7)	-1.2 (2.0)	-0.4 (2.2)	-5.0 (2.3)	-3.7 (2.4)
2	-5.4 (2.6)	-4.0 (2.7)	-4.2 (2.1)	-3.2 (2.2)	-6.2 (2.4)	-4.6 (2.5)
10	-0.2 (2.1)	0.0 (2.3)	-1.2 (2.9)	-0.9 (2.7)	-2.8 (1.9)	-2.2 (1.9)
46.4	-3.4 (2.8)	-3.0 (2.8)	-2.9 (3.6)	-2.2 (3.7)	-3.1 (2.6)	-1.5 (2.7)
100	-9.7 (6.0)	-4.7 (6.4)	-29.6 (24.2)	-12.2 (26.6)	-11.8 (6.5)	-5.8 (7.0)

Table 2: Stratospheric ozone trends with 2σ uncertainties (in % per decade) from SWOOSH during 1998-2020 based on OLS and Ridge regression.

Levels (hPa)	60-35°S		20°S-20°N		35-60°N	
	OLS	Ridge	OLS	Ridge	OLS	Ridge
1	0.0 (1.2)	-0.2 (1.2)	-0.2 (0.9)	-0.1 (1.0)	0.1 (1.0)	-0.2 (1.1)
2	1.5 (1.2)	0.9 (1.2)	1.6 (1.0)	1.1 (1.0)	1.7 (1.1)	1.1 (1.1)
10	0.6 (1.0)	0.3 (1.0)	0.6 (1.5)	0.1 (1.2)	0.3 (0.8)	0.1 (0.9)
46.4	-0.3 (1.3)	-0.3 (1.3)	-1.8 (1.7)	-1.7 (1.7)	-0.3 (1.2)	-0.4 (1.2)
100	0.4 (2.7)	0.0 (2.9)	-15.4 (11.1)	-6.1 (12.0)	-3.8 (2.9)	-1.6 (3.2)

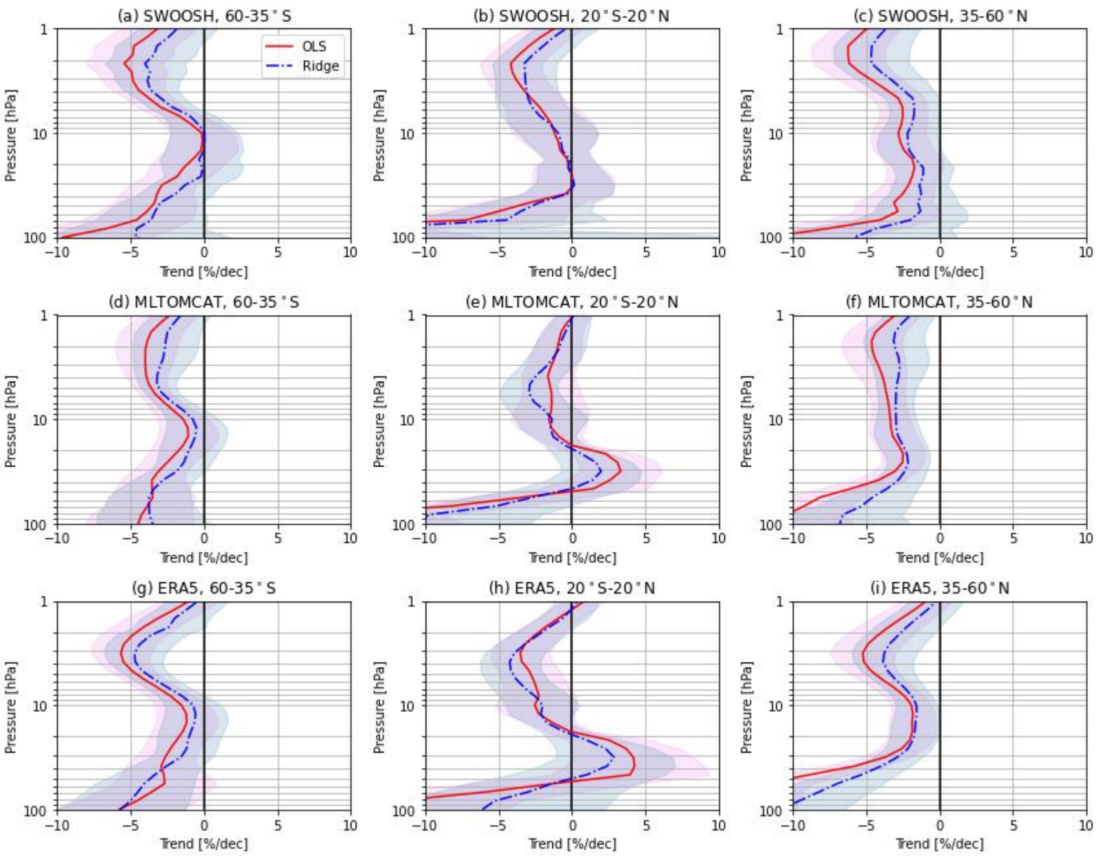

Figure 2: Profiles of annual mean stratospheric ozone trends (% per decade) derived from OLS and Ridge regression methods for three latitude bands (60-35°S, 20°S-20°N and 35-60°N) from (a-c) SWOOSH, (d-f) ML-TOMCAT, and (g-i) model simulation ERA5 over the period 1984-1997. Shaded regions indicate 2-σ uncertainties.

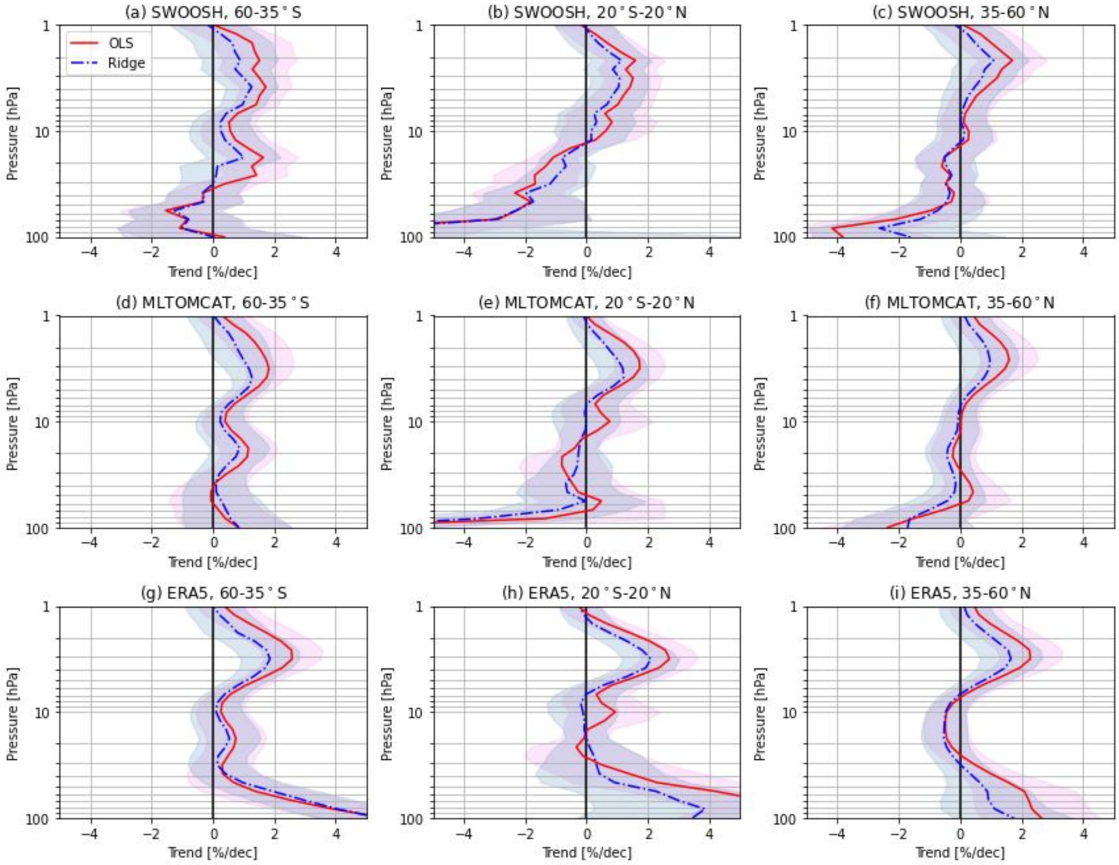

Figure 3: Same as Figure 2 but for the post-1998 time period (1998-2020).

As shown in **Figure 3**, upper stratospheric ozone has increased since 1998 across all three latitude bands and the increases based on Ridge regression are slightly smaller. **Table 2** gives some trend results and corresponding 2-σ uncertainties from SWOOSH data during 1998-2020. The significant positive ozone trends (~2 % per decade for OLS regression) in the upper stratosphere are consistent with the statistically significant trends shown in previous studies (Ball et al., 2017; Sofieva et al., 2017; Steinbrecht et al., 2017; Bourassa et al., 2018; WMO, 2018; Petropavlovskikh et al., 2019; Godin-Beekmann et al., 2022; Bognar et al., 2022). The largest increase based on Ridge regression is 1.1±1.1 % per decade near 2 hPa at NH mid-latitudes, 1.1±1.0 % per decade near 2 hPa in the tropics, and 1.3±0.8 % per decade at 3.8 hPa at SH mid-latitudes. In the mid- and lower stratosphere, ozone trends are generally negative except for the non-significant positive trends near 20 hPa at SH mid-latitudes where a large difference of ~1.3 % per decade occurs between OLS and Ridge regression methods. Negative trends with larger uncertainties are observed in the lower stratosphere, which are most pronounced in the tropics (-6.1±12.0 % per decade at 100 hPa), followed by the decrease at NH mid-latitudes (-1.6±3.2 % per decade at 100 hPa). The largest difference between OLS and Ridge regression methods occurs in the tropical lowermost stratosphere with a difference of ~9 % per decade at 100 hPa (but with larger uncertainties >10 % per decade for both regression methods), followed by the NH mid-latitudes with >2 % per decade difference at 100 hPa (~3 % per decade uncertainties). Note that, despite the large differences between OLS and Ridge-based trends, they are still within the uncertainties of the individual trends. The observed ozone decreases in the lower stratosphere are similar to recent records (e.g. Ball et al., 2019; 2020; Godin-Beekmann et al., 2022), which could be explained by the increased tropical upwelling and mid-latitude mixing (Wargan et al., 2018; Ball et al., 2020; Orbe et al., 2020; Davis et al., 2023). Nevertheless, the modelled lower stratospheric trends do not match those derived from observations.

Compared to the trend estimates from simulation ERA5 in **Figure 3**, the ML-TOMCAT data set shows more consistent results with the SWOOSH data, with negative ozone trends in the tropical and NH mid-latitude lower stratosphere. The better agreement between ML-TOMCAT and SWOOSH, due to satellite corrections derived from the same MLS measurements, shows some improvements in this machine-learning based data set compared to the TOMCAT CTM. The largest differences between SWOOSH- and ML-TOMCAT-based ozone trends appear in the SH mid-latitude lower stratosphere where ML-TOMCAT shows positive trends, and in the tropical mid- and lower stratosphere with close to zero trends near 60 hPa (although these trends have large uncertainties). On the other hand, trends from model simulation ERA5 show largest inconsistencies with respect to SWOOSH-based trends in the lower stratosphere. Simulation ERA5 shows positive trends for all three latitude bands but they are more pronounced in the SH mid-latitudes (5.4±2.0 % per decade at 100 hPa for Ridge regression). These differences between satellite-based datasets and model simulation suggest there are still large uncertainties in the lower stratosphere where dynamical processes dominate (Dietmüller et al., 2021; Li et al., 2022). Ball et al. (2020) reported significant discrepancies in observation-model lower stratospheric ozone trends by using various satellite-based data sets and chemistry–climate models (CCMs). Although the inconsistencies vary with various datasets and fit methods (Dietmüller et al., 2021; Bognar et al., 2022), models generally do not reproduce the observations and the reason for this remains an open question.

Similar to SWOOSH-derived trends, the Ridge-based trends from ML-TOMCAT and simulation ERA5 are smaller in magnitude when compared to OLS-based trends. An evident OLS-Ridge difference appears at near 10 hPa in the tropical stratosphere where OLS-based trends from both ML-TOMCAT and simulation ERA5 show a small peak (~1 % per decade) but Ridge-based trends are close to zero. This difference between OLS and Ridge regression might be associated with the regression methods and correction used for the autoregression (AR1). Although the AR1 correction is applied to OLS regression, we should be aware of the limitations of the Cochrane-Orcutt method, e.g., it is specifically designed to handle first-order autocorrelation (AR1). If the autocorrelation in the residuals follows a higher-order AR process or a different pattern, this method may not be appropriate or effective. Besides, the estimated regression coefficients and their interpretation can be affected for the corrected model with the application of the Cochrane-Orcutt method.

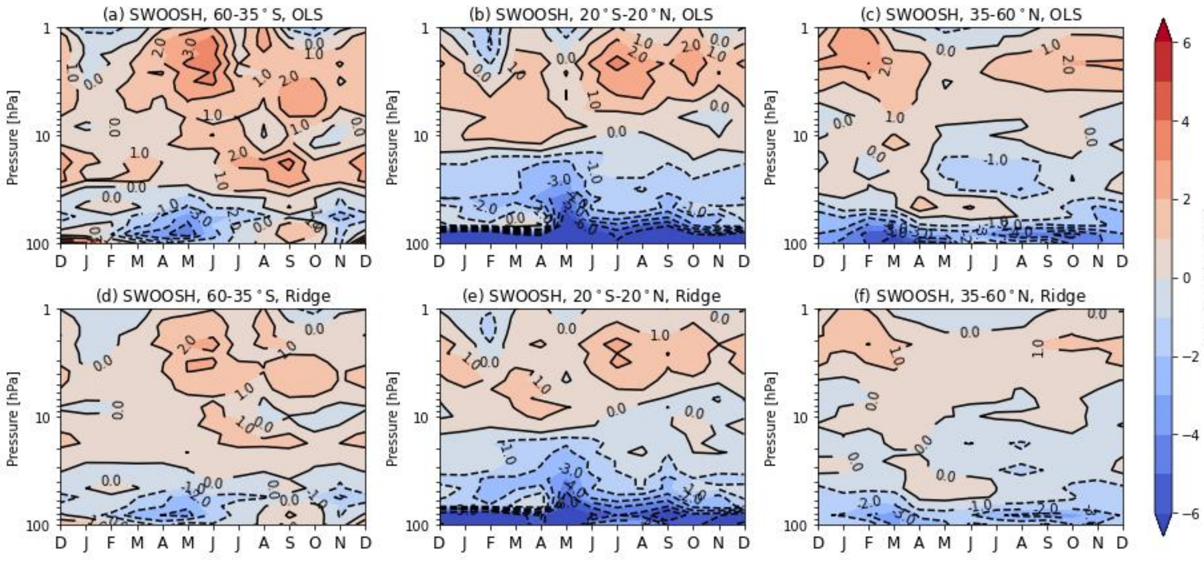

Figure 4: Pressure-season variation of linear trends in ozone (% per decade) from SWOOSH data over 1998–2020 for three selected latitudinal bands (60-35°S, 20°S-20°N, 35-60°N) based on (a-c) OLS and (d-f) Ridge regression methods.

The seasonal variations of stratospheric ozone trends from SWOOSH data during 1998-2020 are averaged over three latitude bands (60-35°S, 20°S-20°N, 35-60°N) and compared using both OLS and Ridge regression methods, as shown in **Figure 4**. There is a strong seasonal dependence in stratospheric ozone trends, with the signs of positive and negative trends varying with season and altitude. OLS-based trend estimates are in good agreement with those in previous studies (e.g. Szelag et al., 2020). Positive trends are observed in the upper stratosphere (10-1 hPa) for almost all seasons with the maximum (>2 % per decade) in local winter at mid-latitudes, while in the tropics (near 1-3 hPa) negative trends of more than -1% per decade appear in December-January-February (DJF). In the middle stratosphere (32-10 hPa), there is a hemispheric asymmetric structure with positive trends (1-2 % per decade) in the SH mid-latitudes and negative trends (-1 % per decade) in the NH mid-latitudes in June-July-August (JJA). In the lower stratosphere (100-32 hPa), there are persistent negative trends for all seasons in the tropics with the largest negative trends in May (< -4% per decade) and negligible trends in March and April near 60 hPa. Trends in the NH mid-latitudes are more negative in the lowermost stratosphere compared to those in the SH mid-latitudes. In the SH mid-latitudes, there exists a clear transition from negative trends in February-July to positive trends in August-October. The Ridge regression method shows very similar results to those in OLS except that the absolute Ridge-based trends and fit coefficients are smaller.

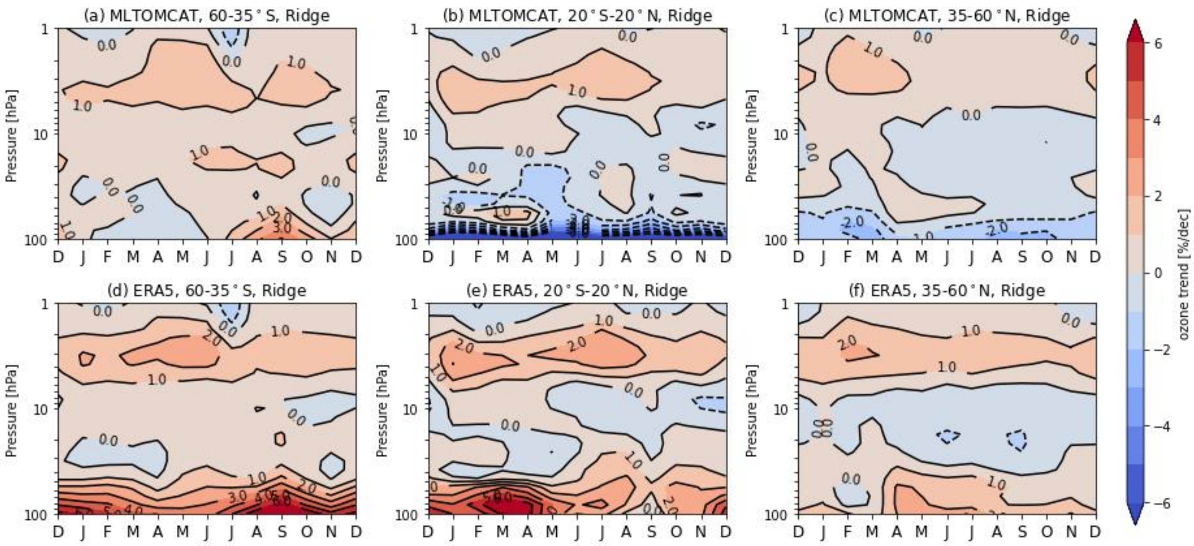

Figure 5: Pressure-season variation of linear trends in ozone (% per decade) from (a-c) ML-TOMCAT and (d-f) simulation ERA5 over 1998–2020 for three selected latitudinal bands (60-35°S, 20° S-20°N, 35-60°N) based on the Ridge regression method.

Figure 5 shows the comparison of seasonal variations of stratospheric ozone trends over the post-1998 period from ML-TOMCAT data and model simulation ERA5 based on the Ridge regression. Trends from ML-TOMCAT data show a more consistent seasonal dependence with those from SWOOSH data, while model-based estimates show significant differences. In the SH lowermost stratosphere, simulation ERA5 shows positive trends for all seasons, which is different from the trend pattern with seasonal dependence from SWOOSH and ML-TOMCAT data. In the tropical mid- and lower stratosphere, there are large differences in seasonal ozone trends between model simulation and satellite data. Trends from simulation ERA5 show more positive trends for all seasons in the tropical lower stratosphere, opposite to the negative trends from SWOOSH and ML-TOMCAT. Also, simulation ERA5 shows more significant positive trends in the tropical lowermost stratosphere during winter and spring compared to ML-TOMCAT. In the NH lower stratosphere, the negative trends from ML-TOMCAT show better agreement with those from SWOOSH while simulation ERA5 still shows opposite and weak positive trends in most months. The reason for the better agreement between ML-TOMCAT and SWOOSH-based trend estimates may be from the fact that denser MLS measurements that are part of SWOOSH are also used for the training of ML-TOMCAT model. These seasonal trends provide more information beyond the annual mean trends, which is helpful in further understanding the role of dynamical variability in short-term trends as well as the prediction of ozone recovery.

The post-1998 seasonal ozone profile trends averaged over the three latitude bands (60-35°S, 20°S-20°N, 35-60°N) from SWOOSH, ML-TOMCAT and simulation ERA5 are presented and compared in **Figure S3** with Ridge regression. The differences of the seasonal ozone profile trends using OLS and Ridge regression methods are also shown in **Figure S4**.

Consistent with the monthly mean trend variations shown in **Figures 4-5**, the ozone profile trends during post-1998 time periods show seasonal and altitude dependence for all data sets. The ML-TOMCAT data set shows similar seasonal trends to those using SWOOSH data, while model simulation ERA5 shows larger inconsistencies especially in the lower stratosphere. The considerable differences suggest that there is a large degree of uncertainty in the estimates of seasonal ozone trends, particularly in the lower stratosphere, where dynamical processes dominate, in addition there is larger uncertainties in the satellite data. Therefore, caution is needed when discussing the results for this region, as neither regression method can reliably capture the large variability.

As shown in **Figure S4**, the positive trends at SH mid-latitudes in the middle stratosphere (near 20-30 hPa) from SWOOSH data are constrained by ~2 % per decade in September-October-November (SON) with Ridge regression. Meanwhile, the negative trends in the NH mid-latitudes in JJA are also constrained by ~0.7 % per decade compared to OLS regression. In the tropical lowermost stratosphere (near 100 hPa), the observed negative trends are constrained with Ridge regression by more than 2 % per decade for all seasons. For ML-TOMCAT and simulation ERA5, trends in the tropical lower stratosphere also show large differences with a wide variability for different seasons. Despite these differences between OLS- and Ridge-based ozone profile trends, the even larger uncertainties, e.g. in the lower stratosphere (**Figure S3**), suggest the ozone trends from the two regression models are not different from each other.

4.2 Ozone variations associated with natural processes

The QBO at 30 hPa and 50 hPa are important proxies used in the regression model to represent the variability of stratospheric ozone in the tropics as well as at higher latitudes (Anstey and Shepherd, 2014; Lu et al., 2019; Xie et al., 2020; Zhang et al., 2021; Wang et al., 2022). **Figures 6-7** show the seasonal responses of stratospheric ozone to QBO at 30 hPa and 50 hPa from SWOOSH, ML-TOMCAT and simulation ERA5 over the long period 1984–2020 based on Ridge regression. Similar results based on OLS regression are also presented in the supplementary **Figures S5-6**. It is obvious that the seasonal cycle modulates the QBO at higher latitudes with more significant responses during local winter-spring (Tung and Yang, 1994; Wang et al., 2022). A double-peaked vertical structure of stratospheric ozone anomalies associated with QBO is also clear in the tropics for all seasons. All data sets show very consistent influences of QBO on ozone, however, there exist large seasonal QBO pattern differences between various data sets. In the mid-latitude lower stratosphere, model simulation ERA5 shows more negative ozone anomalies from the two QBO phases in all seasons compared to SWOOSH and ML-TOMCAT. In the tropics, there are more positive ozone responses to QBO in simulation ERA5 at near 30 hPa for all seasons (**Figure 6h**) as well as below 50 hPa in DJF (**Figure 7h**) when compared to ML-TOMCAT. The positive QBO influences on the tropical ozone and negative influences in the subtropical region are associated with the QBO phase changing from the Equator to the subtropics, which is consistent with previous studies of QBO signals in total column ozone (Tung and Yang, 1994; Chehade et al., 2014; Li et al., 2022).

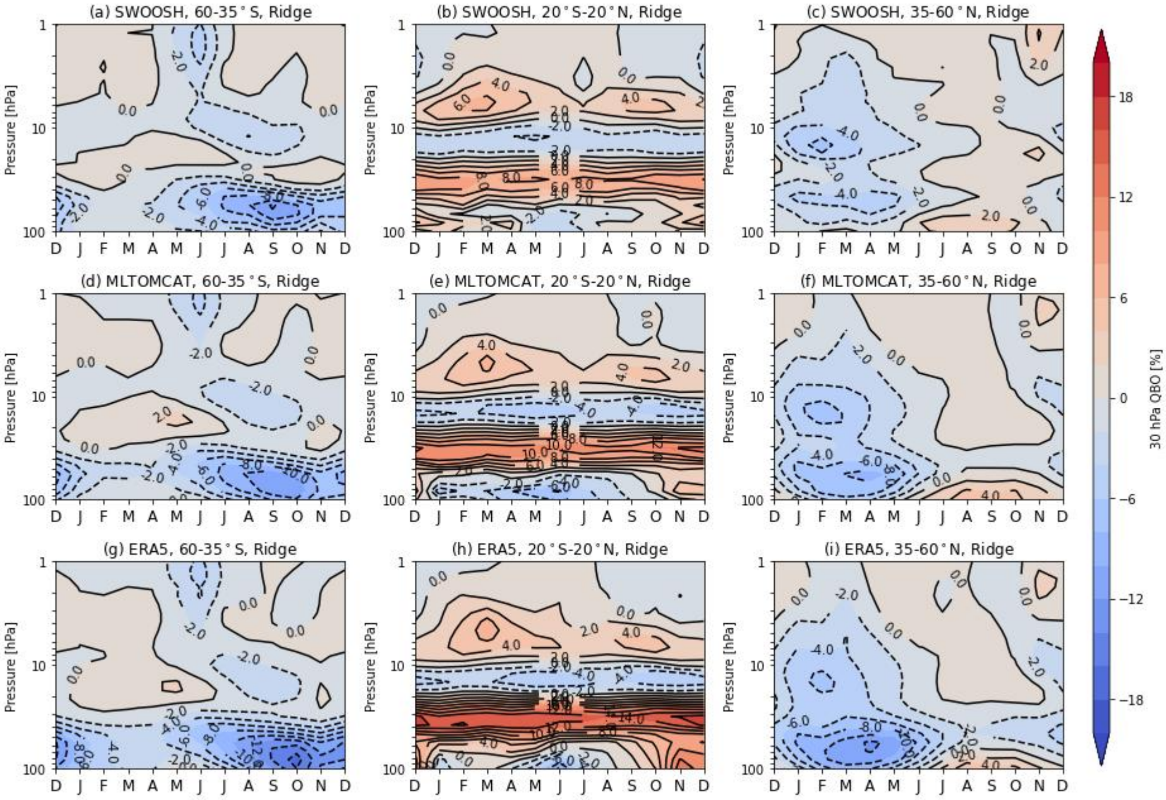

Figure 6: Pressure-season variation of the 30 hPa QBO response in ozone (%) from (a-c) SWOOSH, (d-f) ML-TOMCAT, (g-i) simulation ERA5 for three selected latitudinal bands (60-35°S, 20° S-20°N, 35-60°N) based on the Ridge regression method.

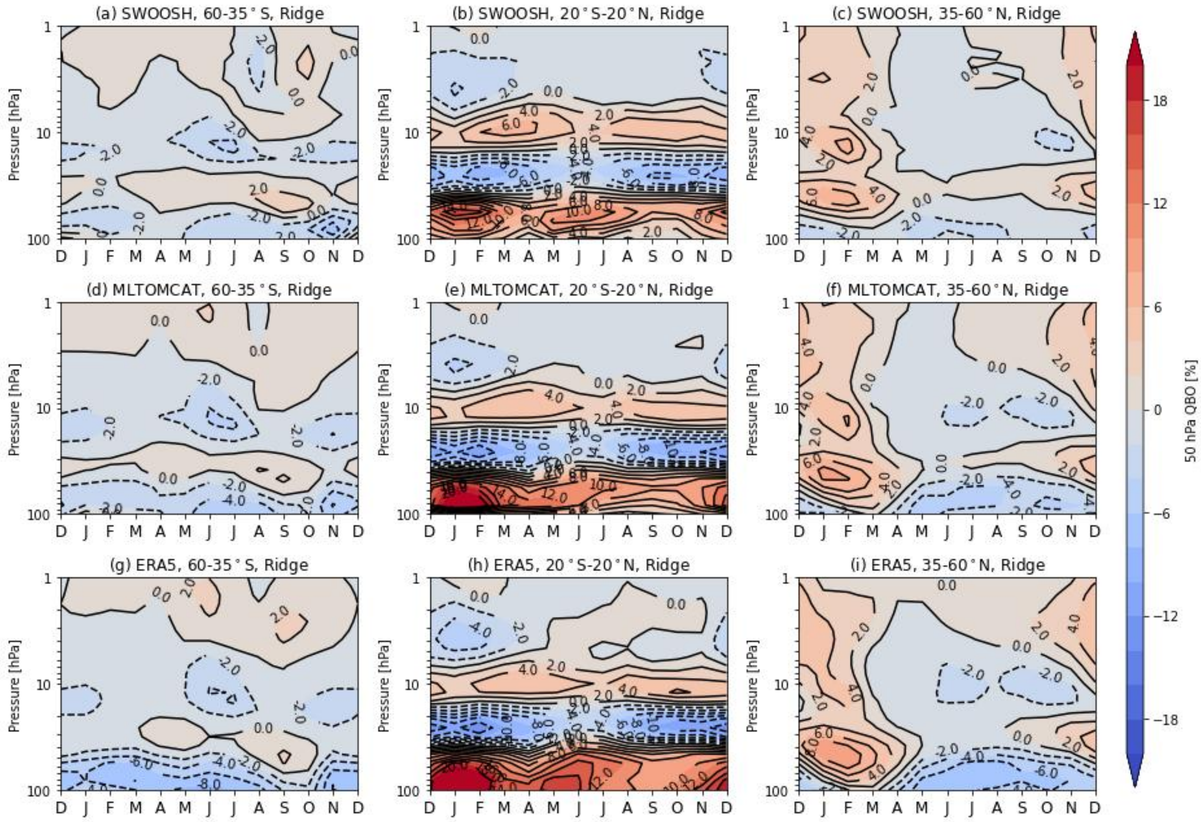

Figure 7: Same as Figure 6 but for the 50 hPa QBO response in ozone (%).

Figure 8 shows the solar cycle response in stratospheric ozone variations derived from SWOOSH, ML-TOMCAT and simulation ERA5 based on OLS and Ridge regression methods. Similar to the trend results, the coefficients of solar cycle ozone response from Ridge regression are relatively smaller in magnitude. Besides, The OLS-based solar response from SWOOSH data displays a U-shaped structure in the upper stratosphere with maxima stretching from the tropics (5-10 hPa) to mid-latitudes (1-3 hPa). A significant negative peak is observed near 30 hPa in the tropics, which is also found in ML-TOMCAT and simulation ERA5 (although not statistically significant). The U-shaped structure in the upper stratosphere is not well reproduced by ML-TOMCAT and simulation ERA5 as the solar cycle ozone response is overestimated at most latitudes and pressure levels, while the locations of the maximum solar responses in the tropics and mid-latitudes are consistent. Differences between the OLS- and Ridge-based solar response include (1) the location of the maximum solar cycle ozone response in the tropical upper stratosphere (which is near 3-5 hPa for Ridge regression), (2) the location of the negative peak solar response in the tropics (which is up to ~10 hPa for all data sets in Ridge regression), and (3) the significant solar signals near 30-50 hPa in the NH extratropics (which is absent from Ridge regression). These features show many similarities as well as differences when compared to those in previous observations and model simulations (Soukharev and Hood, 2006; Maycock et al., 2018; Ball et al., 2019; Dhomse et al., 2022). The fact is that estimates of a realistic solar cycle signal are challenging as they are not only dependent on the chosen data set, but also associated with the regression methods, model setup, and proxies used in the MLR analysis (Smith & Matthes, 2008; Chiodo et al., 2014; Ball et al., 2016).

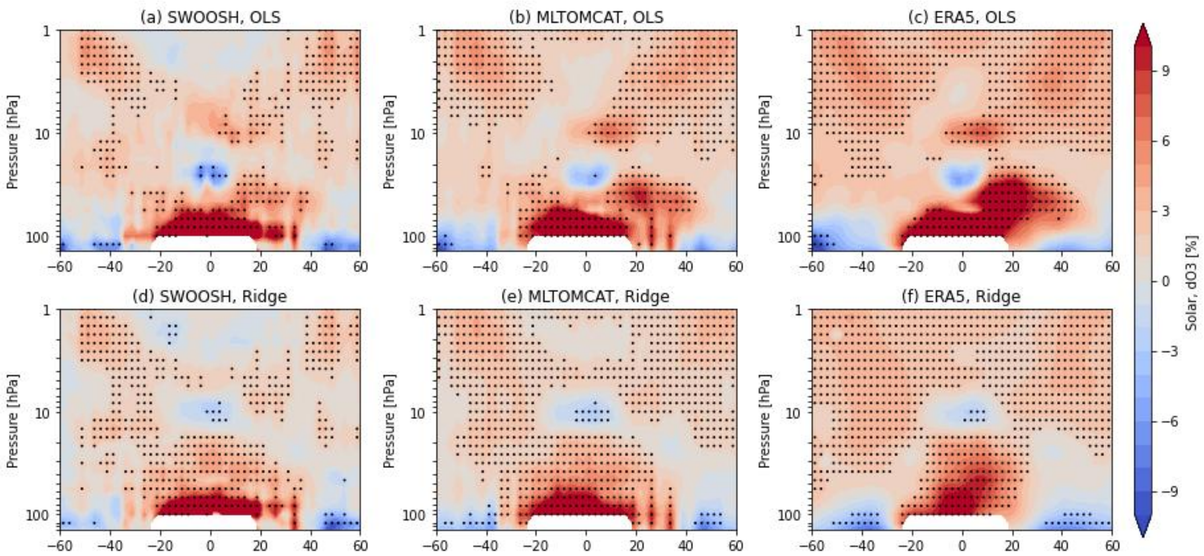

Figure 8: Latitude-pressure cross sections of solar cycle response in stratospheric ozone (%) derived from SWOOSH, ML-TOMCAT, and TOMCAT simulation ERA5 based on (a-c) OLS and (d-f) Ridge regression methods. The stippling indicates regions that are significant at the 95 % level.

The solar response in tropical stratospheric ozone (20°S-20°N) is quantified and compared based on different data sets with OLS and Ridge regression methods, as shown in **Figure 9**. The OLS-based solar response profile from SWOOSH shows a single and broad peak response (2.8 %) at 10 hPa, which is consistent with the results of Ball et al. (2019). The Ridge-based profile shows a different structure with a significant peak signal (1.5 %) near 4.6 hPa and an insignificant negative signal near 10 hPa. In the tropical lower stratosphere there is a secondary ozone peak for both OLS- and Ridge-based response, which has been reported in previous studies and thought to be a dynamical response to the solar cycle (Dhomse et al., 2016). ML-TOMCAT and simulation ERA5 display a consistent structure with SWOOSH although they overestimate the peak response as well as the signals in the upper stratosphere (above 2 hPa). Again, the differences between OLS- and Ridge-based SCS profiles indicate that how the MLR model is applied may play a role in the appearance of the solar cycle ozone response (Smith and Matthes, 2008).

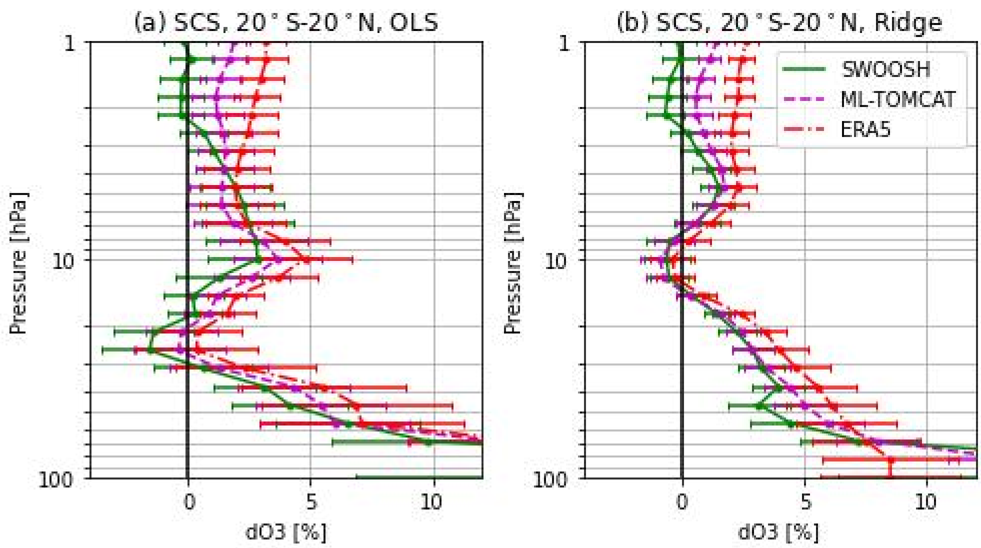

Figure 9: Profiles of ozone solar cycle signal (SCS) for the tropical region (20°S–20°N) from SWOOSH, ML-TOMCAT as well as TOMCAT simulation ERA5 based on (a) OLS and (b) Ridge regression methods. Error bars are 2σ uncertainties.

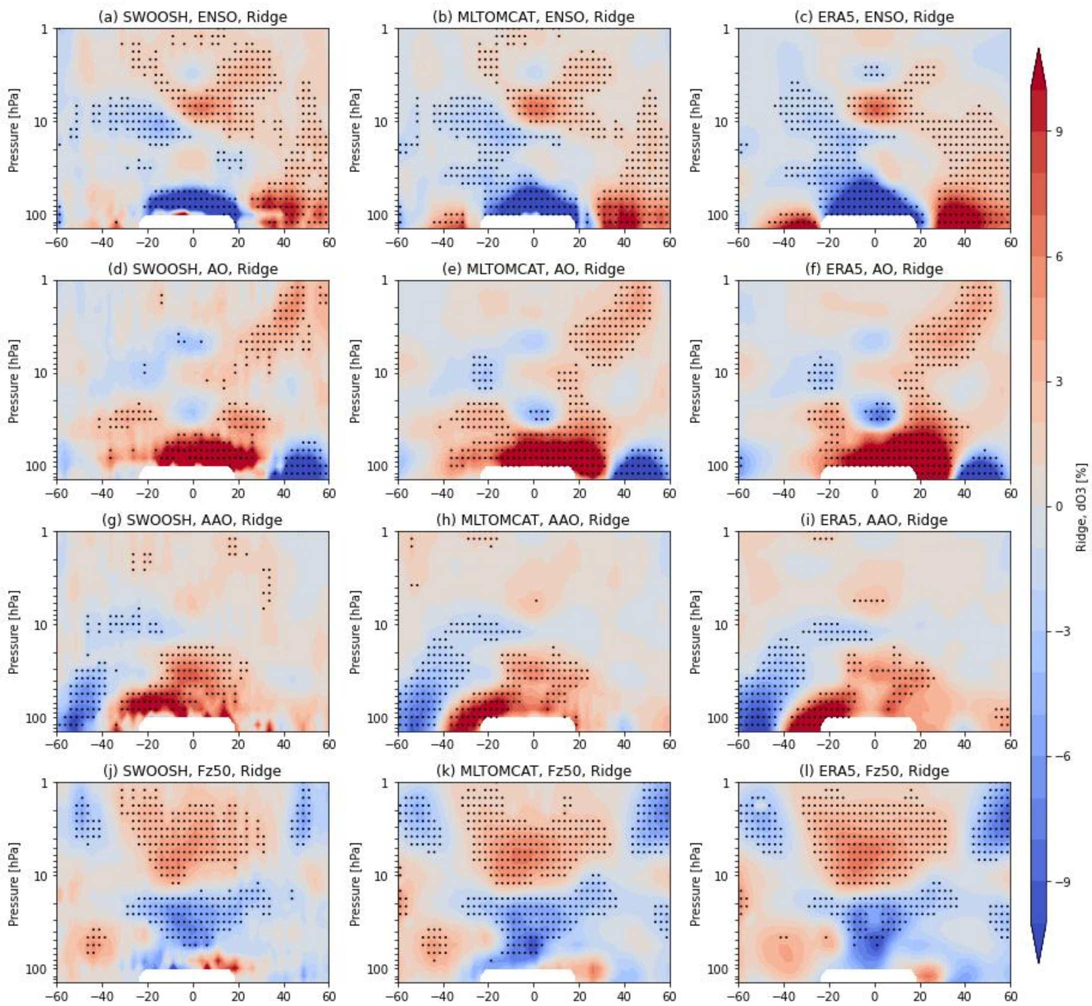

Figure 10: Latitude-pressure cross sections of the natural ozone variations (%) associated with (a-c) ENSO, (d-f) AO, (g-i) AAO and (j-l) EP flux (Fz50) derived from SWOOSH, ML-TOMCAT, and simulation ERA5 based on the Ridge regression method. The stippling indicates regions that are significant at the 95 % level.

In addition, ozone variations associated with natural processes (ENSO, AO, AAO and EP flux) based on different data sets are shown in **Figure 10** with Ridge regression. The ENSO coefficient indicates a significant negative influence on the tropical lower stratospheric ozone, while there are positive patterns in the northern mid-high latitudes due to enhanced transport from the tropics during warm ENSO events (Frossard et al., 2013; Rieder et al., 2013). In the southern mid-latitudes, the ENSO coefficients are statistically insignificant, implying that ENSO-related ozone variations differ by hemisphere with the ENSO phase (Ziemke et al., 2010; Oman et al., 2013).

The negative phase of AO (AAO) in the northern (southern) extratropics leads to increased ozone with enhanced ozone transport (Steinbrecht et al., 2011; Chehade et al., 2014). These negative AO (AAO) indices in the extratropics are characterized by a pronounced poleward deflection of planetary waves, which means an enhanced Brewer-Dobson circulation and more ozone transport into the extratropics (Steinbrecht et al., 2011). As shown in **Figure 10**, zonally averaged ozone variations in the lower stratosphere are more sensitive to the AO and AAO indices compared to those in the middle and upper stratosphere.

Changes in the vertical component (Fz) of the stratospheric EP flux represents the ozone transport due to variations in planetary wave driving from the troposphere into the stratosphere (Fusco and Salby, 1999; Weber et al., 2003; Dhomse et al., 2006). In the tropics, the strengthened upward transport is linked to an upward shift of the maximum ozone mixing ratio in the middle stratosphere, as a result there are two cells of opposite ozone pattern near 10 hPa. A similar pattern appears at mid-latitudes due to enhanced transport by the stratospheric residual circulation. The out-of-phase between the tropics and mid-latitudes reflects the overturning Brewer-Dobson circulation (Randel et al., 2002). In the lower stratosphere, the hemispherical asymmetric ozone pattern could potentially result from the combination of changes in chemical and dynamical processes (Banerjee et al., 2016; Abalos et al., 2017).

Both satellite data and model simulation capture these features, although there are still some differences. In the lower stratosphere, simulation ERA5 overestimates the positive ENSO response in the extratropics than ML-TOMCAT does. In the tropical middle stratosphere near 30 hPa, again ERA5 shows larger AO-related responses than SWOOSH or ML-TOMCAT. **Figure S7** shows the results from OLS regression for comparison. With the correction for AR1 applied to OLS regression, the uncertainties of the fit coefficients for these dynamical proxies increase, which makes most of the contributions statistically insignificance. As the correction method can also change the estimated regression coefficients, the differences between OLS- and Ridge-based results should be considered with care. As a caveat, the regression fit has been improved by accounting for various dynamical proxies, however, these proxies are not independent and they can only partly explain the complicated structure of dynamical variability (Petropavlovskikh et al., 2019; WMO, 2022). Thus, the use of these dynamical proxies requires care, especially for the lower stratospheric region.

5 Summary and Conclusions

In this study, we have investigated stratospheric ozone trends and their attribution with ordinary (OLS) and regularised (Ridge) multivariate regression methods. The merged satellite-based data set (SWOOSH), TOMCAT model simulation forced with ERA5 reanalysis data as well as a machine-learning-based satellite-corrected TOMCAT product (ML-TOMCAT) are used and compared over the period 1984-2020. We adopt the Ridge regression method to overcome the issue of over-fitting due to the complex coupling in many atmospheric processes. We have analyzed the ozone profile trends and ozone variations associated with natural processes based on both OLS and Ridge regression methods. Our main results are summarized as follows:

- As shown in Section 4, estimated ozone trends from the OLS- and Ridge-based regression models show significant differences. With a penalty considered in Ridge regression, coefficients in the regression model are shrunk to a certain extent which is determined by the optimal tuning value. This optimal tuning value changes with altitude and latitude, indicating, as expected, that ozone concentrations are controlled by different processes at different altitudes and latitudes and it is inappropriate to use the same tuning value to the Ridge regression model for all locations. To avoid over-fitting-related issues, we have applied Ridge regression to quantify the stratospheric ozone trends and changes and to compare it with the conventional OLS regression method.

- We compare the stratospheric ozone profile trends for the pre- and post-1998 periods as well as the seasonal dependence with OLS and Ridge regression. Both OLS and Ridge regression methods show a strong seasonal dependence in stratospheric ozone trends. Trend estimates at different altitudes and seasons are constrained by Ridge regression in magnitudes and fluctuations. For example, ozone declines during 1984-1997 are smaller in Ridge regression, and largest differences between ozone trends using OLS and Ridge regression are apparent in the upper stratosphere (~1 % per decade at 2 hPa) and the lowermost stratosphere (>4 % per decade at 100 hPa) for SWOOSH data. Since 1998, all the datasets confirm stratospheric ozone recovery in the upper stratosphere but there are differences in the magnitudes and the locations. In the NH mid-latitudes and the tropics, largest positive trends are observed at 2 hPa (1.1 ± 1.1 % per decade and 1.1 ± 1.0 % per decade, respectively). On the other hand, positive trends are somewhat larger at SH mid-latitudes (1.3 ± 0.8 % per decade) though they occur at 3.8 hPa. Negative trends with large uncertainties are observed in the lower stratosphere and are most pronounced in the tropics. The largest difference between OLS and Ridge regression methods appears in the tropical lower stratosphere (with ~9 % per decade difference at 100 hPa), but it is within the uncertainties of the individual trends (>10 % per decade). Comparing trend estimates from TOMCAT model simulation, we find that ML-TOMCAT trends are more consistent with those using SWOOSH data. The differences between satellite-based datasets and model simulations suggest there are still large uncertainties in the lower stratosphere where dynamical processes dominate.
- Ozone variations associated with natural processes such as QBO, solar variability, ENSO, AO, AAO and EP flux indicate that Ridge regression shrinks the regression coefficients as some of the explanatory variables are co-related. The differences between OLS- and Ridge-based results are associated with how the MLR model is applied and should be considered with care. Despite the differences in regression coefficients and statistical significance, there are similar characteristics in natural ozone variations for both regression methods. For example, the positive QBO influences on the tropical lower stratospheric ozone and negative influences in the subtropical region are consistent with QBO signals in total column ozone. The stratospheric ozone solar cycle response shows a U-shaped spatial structure in the upper stratosphere. The enhanced transport from the tropics during warm ENSO events leads to a significant negative influence on the tropical lower stratospheric ozone and positive influences in the northern mid-high latitudes. The negative phase of AO/AAO in the northern/southern extratropics leads to increased ozone with enhanced ozone transport. The stratospheric EP flux represents planetary wave driving from the troposphere into the stratosphere and affects the ozone transport through Brewer-Dobson circulation. Again, ML-TOMCAT shows more consistent results with those using SWOOSH data while simulation ERA5 shows larger inconsistencies especially in the lower stratosphere.

Finally, we argue that the considerable differences between the satellite data and model simulations highlight the large uncertainties in our understanding about the lower stratospheric trends, which suggests that caution is needed while interpreting results with different methodologies and data sets.

Data availability. SWOOSH data is available from https://csl.noaa.gov/groups/csl8/swoosh/. ML-TOMCAT data is available via https://doi.org/10.5281/zenodo.5651194. The model data are available at https://doi.org/10.5281/zenodo.6988615 (Li et al., 2022, last access: Mar 2023). Climate data used in this study are available at the source and references in Sect. 2 and Sect. 3.

Author contributions. YL performed the data analysis and prepared the manuscript. SSD, MPC and WF performed the model simulations. SSD, MPC, WF, JB, YX and DG gave support for the discussion, simulation and interpretation and helped to write the paper. All authors edited and contributed to subsequent drafts of the paper.

Competing interests. The authors declare that they have no conflicts of interest.

Acknowledgements. The modelling work is supported by National Centre for Atmospheric Science (NCAS). We thank all providers of the climate data used in this study. The model runs were performed on the Leeds ARC and UK Archer2 HPC facilities.

Financial Support. This work was supported by the Second Tibetan Plateau Scientific Expedition and Research Program (2019QZKK0604) and by the NERC LSO3 project (NE/V011863/1). We also acknowledge the support of the National Natural Science Foundation of China (grant no. 42192512, 2022YFF0801703) and the Natural Science Foundation for universities in Jiangsu province (grant no. 21KJB510007).

References

Abalos, M., Randel, W. J., Kinnison, D. E., and Garcia, R. R.: Using the Artificial Tracer e90 to Examine Present and Future UTLS Tracer Transport in WACCM, J Atmos Sci, 74, 3383-3403, https://doi.org/10.1175/JAS-D-17-0135.1, 2017.

Anderson, J., Russell, J. M., Solomon, S., and Deaver, L. E.: Halogen Occultation Experiment confirmation of stratospheric chlorine decreases in accordance with the Montreal Protocol, J. Geophys. Res.-Atmos., 105, 4483–4490, https://doi.org/10.1029/1999JD901075, 2000.

Anstey, J. A. and Shepherd, T. G.: High-latitude influence of the quasi-biennial oscillation, Q. J. Roy. Meteor. Soc., 140, 1–21, https://doi.org/10.1002/qj.2132, 2014.

Banerjee, A., Maycock, A. C., Archibald, A. T., Abraham, N. L., Telford, P., Braesicke, P., and Pyle, J. A.: Drivers of changes in stratospheric and tropospheric ozone between year 2000 and 2100, Atmos. Chem. Phys., 16, 2727–2746, https://doi.org/10.5194/acp-16-2727-2016, 2016.

Ball, W. T., Alsing, J., Mortlock, D. J., Rozanov, E. V., Tummon, F., and Haigh, J. D.: Reconciling differences in stratospheric ozone composites, Atmos. Chem. Phys., 17, 12269–12302, https://doi.org/10.5194/acp-17-12269-2017, 2017.

Ball, W. T., Alsing, J., Mortlock, D. J., Staehelin, J., Haigh, J. D., Peter, T., Tummon, F., Stübi, R., Stenke, A., Anderson, J., Bourassa, A., Davis, S. M., Degenstein, D., Frith, S., Froidevaux, L., Roth, C., Sofieva, V., Wang, R., Wild, J., Yu, P., Ziemke, J. R., and Rozanov, E. V.: Evidence for a continuous decline in lower stratospheric ozone offsetting ozone layer recovery, Atmos. Chem. Phys., 18, 1379–1394, https://doi.org/10.5194/acp-18-1379-2018, 2018.

Ball, W. T., Alsing, J., Staehelin, J., Davis, S. M., Froidevaux, L., and Peter, T.: Stratospheric ozone trends for 1985–2018: sensitivity to recent large variability, Atmos. Chem. Phys., 19, 12731–12748, https://doi.org/10.5194/acp-19-12731-2019, 2019 a.

Ball, W. T., Rozanov, E. V., Alsing, J., Marsh, D. R., Tummon, F., Mortlock, D. J., Kinnison, D., and Haigh, J. D.: The Upper Stratospheric Solar Cycle Ozone Response, 46, 1831-1841, https://doi.org/10.1029/2018GL081501, 2019 b.

Ball, W. T., Chiodo, G., Abalos, M., Alsing, J., and Stenke, A.: Inconsistencies between chemistry–climate models and observed lower stratospheric ozone trends since 1998, Atmos. Chem. Phys., 20, 9737–9752, https://doi.org/10.5194/acp-20-9737-2020, 2020.

Bognar, K., Tegtmeier, S., Bourassa, A., Roth, C., Warnock, T., Zawada, D., and Degenstein, D.: Stratospheric ozone trends for 1984–2021 in the SAGE II–OSIRIS–SAGE III/ISS composite dataset, Atmos. Chem. Phys., 22, 9553–9569, https://doi.org/10.5194/acp-22-9553-2022, 2022.

Bourassa, A. E., Roth, C. Z., Zawada, D. J., Rieger, L. A., McLinden, C. A., and Degenstein, D. A.: Drift-corrected Odin-OSIRIS ozone product: algorithm and updated stratospheric ozone trends, Atmos. Meas. Tech., 11, 489–498, https://doi.org/10.5194/amt-11-489-2018, 2018.

Chehade, W., Weber, M., and Burrows, J. P.: Total ozone trends and variability during 1979–2012 from merged data sets of various satellites, Atmos. Chem. Phys., 14, 7059–7074, https://doi.org/10.5194/acp-14-7059-2014, 2014.

Chiodo, G., Marsh, D. R., Garcia-Herrera, R., Calvo, N., and García, J. A.: On the detection of the solar signal in the tropical stratosphere, Atmos. Chem. Phys., 14, 5251–5269, https://doi.org/10.5194/acp-14-5251-2014, 2014.

Chipperfield, M. P.: New version of the TOMCAT/SLIMCAT off-line chemical transport model: Intercomparison of stratospheric tracer experiments, Q. J. Roy. Meteor. Soc., 132, 1179–1203, https://doi.org/10.1256/qj.05.51, 2006.

Chipperfield, M. P., Bekki, S., Dhomse, S., Harris, N. R., Hassler, B., Hossaini, R., Steinbrecht, W., Thiéblemont, R., and Weber, M.: Detecting recovery of the stratospheric ozone layer, Nature, 549, 211–218, https://doi.org/10.1038/nature23681, 2017.

Chipperfield, M. P., Dhomse, S., Hossaini, R., Feng, W., Santee, M. L., Weber, M., Burrows, J. P., Wild, J. D., Loyola, D., and Coldewey-Egbers, M.: On the cause of recent variations in lower stratospheric ozone, Geophys. Res. Lett., 45, 5718–5726, https://doi.org/10.1029/2018GL078071, 2018.

Cochrane, D. and Orcutt, G. H.: Application of least squares regression to relationships containing auto-correlated error terms, J. Am. Stat. Assoc., 44, 32–61, https://doi.org/10.2307/2280349, 1949.

Davis, S. M., Rosenlof, K. H., Hassler, B., Hurst, D. F., Read, W. G., Vömel, H., Selkirk, H., Fujiwara, M., and Damadeo, R.: The Stratospheric Water and Ozone Satellite Homogenized (SWOOSH) database: a long-term database for climate studies, Earth Syst. Sci. Data, 8, 461–490, https://doi.org/10.5194/essd-8-461-2016, 2016.

Davis, S., Davis, N., Portmann, R., Ray, E., and Rosenlof, K.: The role of tropical upwelling in explaining discrepancies between recent modeled and observed lower stratospheric ozone trends, EGUsphere [preprint], https://doi.org/10.5194/egusphere-2022-1267, 2022.

Davis, S. M., Davis, N., Portmann, R. W., Ray, E., and Rosenlof, K.: The role of tropical upwelling in explaining discrepancies between recent modeled and observed lower-stratospheric ozone trends, Atmos. Chem. Phys., 23, 3347–3361, https://doi.org/10.5194/acp-23-3347-2023, 2023.

Diallo, M., Riese, M., Birner, T., Konopka, P., Müller, R., Hegglin, M. I., Santee, M. L., Baldwin, M., Legras, B., and Ploeger, F.: Response of stratospheric water vapor and ozone to the unusual timing of El Niño and the QBO disruption in 2015–2016, Atmos. Chem. Phys., 18, 13055–13073,https://doi.org/10.5194/acp-18-13055-2018, 2018.

Dietmüller, S., Garny, H., Eichinger, R., and Ball, W. T.: Analysis of recent lower-stratospheric ozone trends in chemistry climate models, Atmos. Chem. Phys., 21, 6811 – 6837, https://doi.org/10.5194/acp-21-6811-2021, 2021.

Dhomse, S., Weber, M., Wohltmann, I., Rex, M., and Burrows, J. P.: On the possible causes of recent increases in northern hemispheric total ozone from a statistical analysis of satellite data from 1979 to 2003, Atmos. Chem. Phys., 6, 1165–1180, https://doi.org/10.5194/acp-6-1165-2006, 2006.

Dhomse, S. S., Chipperfield, M. P., Feng, W., Ball, W. T., Unruh, Y. C., Haigh, J. D., Krivova, N. A., Solanki, S. K., and Smith, A. K.: Stratospheric O_3 changes during 2001–2010: the small role of solar flux variations in a chemical transport model, Atmos. Chem. Phys., 13, 10113–10123, https://doi.org/10.5194/acp-13-10113-2013, 2013.

Dhomse, S. S., Chipperfield, M. P., Feng, W., Hossaini, R., Mann, G. W., and Santee, M. L.: Revisiting the hemispheric asymmetry in midlatitude ozone changes following the Mount Pinatubo eruption: A 3-D model study, Geophys. Res. Lett., 42, 3038–3047, https://doi.org/10.1002/2015gl063052, 2015.

Dhomse, S. S., Chipperfield, M., Damadeo, R., Zawodny, J., Ball, W., Feng, W., Hossaini, R., Mann, G., and Haigh, J.: On the ambiguous nature of the 11 year solar cycle signal in upper stratospheric ozone, Geophys. Res. Lett., 43, 7241–7249, https://doi.org/10.1002/2016GL069958, 2016.

Dhomse, S. S., Feng, W., Montzka, S. A., Hossaini, R., Keeble, J., Pyle, J. A., Daniel, J. S., and Chipperfield, M. P.: Delay in recovery of the Antarctic ozone hole from unexpected CFC-11 emissions, Nature Commun., 10, 5781, https://doi.org/10.1038/s41467-019-13717-x, 2019.

Dhomse, S. S., Arosio, C., Feng, W., Rozanov, A., Weber, M., and Chipperfield, M. P.: ML-TOMCAT: machine-learning-based satellite-corrected global stratospheric ozone profile data set from a chemical transport model, Earth Syst. Sci. Data, 13, 5711–5729,https://doi.org/10.5194/essd-13-5711-2021, 2021 a.

Dhomse, S. S., Chipperfield, M. P., Feng, W., Arosio, C., Weber, M., and Rozanov, A.: ML-TOMCAT V1.0: Machine-Learning-Based Satellite-Corrected Global Stratospheric Ozone Profile Dataset, Zenodo [data set], https://doi.org/10.5281/zenodo.4997959, 2021 b.

Dhomse, S. S., Chipperfield, M. P., Feng, W., Hossaini, R., Mann, G. W., Santee, M. L., and Weber, M.: A single-peak-structured solar cycle signal in stratospheric ozone based on Microwave Limb Sounder observations and model simulations, Atmos. Chem. Phys., 22, 903–916, https://doi.org/10.5194/acp-22-903-2022, 2022.

Dietmüller, S., Garny, H., Eichinger, R., and Ball, W. T.: Analysis of recent lower-stratospheric ozone trends in chemistry climate models, Atmos. Chem. Phys., 21, 6811–6837, https://doi.org/10.5194/acp-21-6811-2021, 2021.

Feng, W., Chipperfield, M. P., Davies, S., Mann, G. W., Carslaw, K. S., Dhomse, S., Harvey, L., Randall, C., and Santee, M. L.: Modelling the effect of denitrification on polar ozone depletion for Arctic winter 2004/2005, Atmos. Chem. Phys., 11, 6559–6573, https://doi.org/10.5194/acp-11-6559-2011, 2011.

Feng, W., Dhomse, S. S., Arosio, C., Weber, M., Burrows, J. P., Santee, M. L., and Chipperfield, M. P.: Arctic ozone depletion in 2019/20: Roles of chemistry, dynamics and the Montreal Protocol, Geophys. Res. Lett., 48, e2020GL091911, https://doi.org/10.1029/2020GL091911, 2021.

Frossard, L., Rieder, H. E., Ribatet, M., Staehelin, J., Maeder, J. A., Di Rocco, S., Davison, A. C., and Peter, T.: On the relationship between total ozone and atmospheric dynamics and chemistry at midlatitudes – Part 1: Statistical models and spatial fingerprints of atmospheric dynamics and chemistry, Atmos. Chem. Phys., 13, 147–164, https://doi.org/10.5194/acp-13-147-2013, 2013.

Fusco, A. C., and M. L. Salby, Interannual variations of total ozone and their relationship to variations of planetary wave activity, J. Clim., 12, 1619 – 1629, https://doi.org/10.1175/1520-0442(1999)012<1619:IVOTOA>2.0.CO;2, 1999.

Gana, R.: Ridge regression and the Lasso: how do they do as finders of significant regressors and their multipliers?, Communications in Statistics- Simulation and Computation, 51, 5738-5772, https://doi.org/10.1080/03610918.2020.1779295, 2022.

Godin-Beekmann, S., Azouz, N., Sofieva, V. F., Hubert, D., Petropavlovskikh, I., Effertz, P., Ancellet, G., Degenstein, D. A., Zawada, D., Froidevaux, L., Frith, S., Wild, J., Davis, S., Steinbrecht, W., Leblanc, T., Querel, R., Tourpali, K., Damadeo, R., MaillardBarras, E., Stübi, R., Vigouroux, C., Arosio, C., Nedoluha, G., Boyd, I., Van Malderen, R., Mahieu, E., Smale, D., and Sussmann, R.: Updated trends of the stratospheric ozone vertical distribution in the 60° S–60° N latitude range based on the LOTUS regression model , Atmos. Chem. Phys., 22, 11657–11673, https://doi.org/10.5194/acp-22-11657-2022, 2022.

Harris, N. R. P., Hassler, B., Tummon, F., Bodeker, G. E., Hubert, D., Petropavlovskikh, I., Steinbrecht, W., Anderson, J., Bhartia, P. K., Boone, C. D., Bourassa, A., Davis, S. M., Degenstein, D., Delcloo, A., Frith, S. M., Froidevaux, L., Godin-Beekmann, S., Jones, N., Kurylo, M. J., Kyrölä, E., Laine, M., Leblanc, S. T., Lambert, J.-C., Liley, B., Mahieu, E., Maycock, A., de Mazière, M., Parrish, A., Querel, R., Rosenlof, K. H., Roth, C., Sioris, C., Staehelin, J., Stolarski, R. S., Stübi, R., Tamminen, J., Vigouroux, C., Walker, K. A., Wang, H. J., Wild, J., and Zawodny, J. M.: Past changes in the vertical distribution of ozone – Part 3: Analysis and interpretation of trends, Atmos. Chem. Phys., 15, 9965–9982, https://doi.org/10.5194/acp-15-9965-2015, 2015.

Hastie, T., Tibshirani, R., and Friedman, J.: Linear Methods for Regression, in: The Elements of Statistical Learning: Data Mining, Inference, and Prediction, Springer New York, New York, NY, 43-99, https://doi.org/10.1007/978-0-387-84858-7_3, 2009.

Hersbach, H., Bell, B., Berrisford, P., Hirahara, S., Horányi, A., Muñoz-Sabater, J., Nicolas, J., Peubey, C., Radu, R., Schepers, D., Simmons, A., Soci, C., Abdalla, S., Abellan, X., Balsamo, G., Bechtold, P., Biavati, G., Bidlot, J., Bonavita, M., De Chiara, G., Dahlgren, P., Dee, D., Diamantakis, M., Dragani, R., Flemming, J., Forbes, R., Fuentes, M., Geer, A., Haimberger, L., Healy, S., Hogan, R. J., Hólm, E., Janisková, M., Keeley, S., Laloyaux, P., Lopez, P., Lupu, C., Radnoti, G., de Rosnay, P., Rozum, I., Vamborg, F., Villaume, S., and Thépaut, J.-N.: The ERA5 global reanalysis, Q. J. Roy. Meteor. Soc., 146, 1999–2049, https://doi.org/10.1002/qj.3803, 2020.

Hoerl, A. E., and Kennard R. W.: Ridge regression: Biased estimation for nonorthogonal problems, Technometrics, 12 (1), 55–67,https://doi.org/10.1080/00401706.1970.10488634, 1970.

Hu, D., Guan, Z., Liu, M., and Feng, W.: Dynamical mechanisms for the recent ozone depletion in the Arctic stratosphere linked to North Pacific sea surface temperatures, Clim. Dynam., 58, 2663-2679, https://doi.org/10.1007/s00382-021-06026-x, 2022.

Kuhn, M. and Johnson, K.: Over-Fitting and Model Tuning. In: Applied Predictive Modeling, Springer, New York, NY, https://doi.org/10.1007/978-1-4614-6849-3_4, 2013.

Lu, J., Xie, F., Tian, W., Li, J., Feng, W., Chipperfield, M., Zhang, J., and Ma, X.: Interannual variations in lower stratospheric ozone during the period 1984–2016, J. Geophys. Res., 124, 8225–8241, https://doi.org/10.1029/2019JD030396, 2019.

Li, Y., Chipperfield, M. P., Feng, W., Dhomse, S. S., Pope, R. J., Li, F., and Guo, D.: Analysis and attribution of total column ozone changes over the Tibetan Plateau during 1979–2017, Atmos. Chem. Phys., 20, 8627–8639, https://doi.org/10.5194/acp-20-8627-2020, 2020.

Li, Y., Dhomse, S. S., Chipperfield, M. P., Feng, W., Chrysanthou, A., Xia, Y., and Guo, D.: Effects of reanalysis forcing fields on ozone trends and age of air from a chemical transport model, Atmos. Chem. Phys., 22, 10635–10656, https://doi.org/10.5194/acp-22-10635-2022, 2022.

Mahieu, E., Chipperfield, M. P., Notholt, J., Reddmann, T., Anderson, J., Bernath, P. F., Blumenstock, T., Coffey, M. T., Dhomse, S. S., Feng, W., and Franco, B.: Recent Northern Hemisphere stratospheric HCl increase due to atmospheric circulation changes, Nature, 515, 104–107, https://doi.org/10.1038/nature13857, 2014.

Marsh, D. R., Lamarque, J.-F., Conley, A. J., and Polvani, L. M.: Stratospheric ozone chemistry feedbacks are not critical for the determination of climate sensitivity in CESM1 (WACCM), Geophys. Res. Lett., 43, 3928–3934, https://doi.org/10.1002/2016GL068344, 2016.

Maycock, A. C., K. Matthes, S. Tegtmeier, H. Schmidt, R. Thiéblemont, L. Hood, H. Akiyoshi, S. Bekki, M. Deushi, P. Jöckel, O. Kirner, M. Kunze, M. Marchand, D.R, Marsh, M. Michou, D. Plummer, L. E. Revell, E. Rozanov, A. Stenke, Y. Yamashita, and K. Yoshida, The representation of solar cycle signals in stratospheric ozone – Part 2:Analysis of global models, Atmos. Chem. Phys., 18, 11,323–11,343, https://doi.org/10.5194/acp-18-11323-2018, 2018.

Monks, S. A., Arnold, S. R., Hollaway, M. J., Pope, R. J., Wilson, C., Feng, W., Emmerson, K. M., Kerridge, B. J., Latter, B. L., Miles, G. M., Siddans, R., and Chipperfield, M. P.: The TOMCAT global chemical transport model v1.6: description of chemical mechanism and model evaluation, Geosci. Model Dev., 10, 3025-3057, https://doi.org/10.5194/gmd-10-3025-2017, 2017.

Montzka, S. A., Dutton, G. S., Portmann, R. W., Chipperfield, M. P., Davis, S., Feng, W., Manning, A. J., Ray, E., Rigby, M., Hall, B. D., Siso, C., Nance, J. D., Krummel, P. B., Mühle, J., Young, D., O'Doherty, S., Salameh, P. K., Harth, C.

M., Prinn, R. G., Weiss, R. F., Elkins, J. W., Walter-Terrinoni, H., and Theodoridi, C.: A decline in global CFC-11 emissions during 2018−2019, Nature, 590, 428-432, https://doi.org/10.1038/s41586-021-03260-5, 2021.

Oman, L. D., A. R. Douglass, J. R. Ziemke, J. M. Rodriguez, D. W. Waugh, and J. E. Nielsen, The ozone response to ENSO in Aura satellite measurements and a chemistry-climate simulation, J. Geophys. Res., 118, 965–976, https://doi.org/10.1029/2012jd018546, 2013.

Orbe, C., Wargan, K., Pawson, S., and Oman, L. D.: Mechanisms Linked to Recent Ozone Decreases in the Northern Hemisphere Lower Stratosphere, J. Geophys. Res-Atmos., https://doi.org/10.1029/2019JD031631, 2020.

Pedregosa, F., Varoquaux, G., Gramfort, A., Michel, V., Thirion, B., Grisel, O., Blondel, M., Louppe, G., Prettenhofer, P., Weiss, R., Weiss, R. J., Vanderplas, J., Passos, A., Cournapeau, D., Brucher, M., Perrot, M., and Duchesnay, E. J. J. M. L. R.: Scikit-learn: Machine Learning in Python, 12, 2825-2830, 2011.

Petropavlovskikh, I., Godin-Beekmann, S., Hubert, D., Damadeo, R., Hassler, B., and Sofieva, V.: SPARC/IO3C/GAW Report on Long-term Ozone Trends and Uncertainties in the Stratosphere, Tech. rep., SPARC, 9th assessment report of the SPARC project, International Project Office at DLR-IPA, GAW Report No. 241, WCRP Report 17/2018, available at: https://elib.dlr.de/126666/, 2019.

Ploeger, F., Abalos, M., Birner, T., Konopka, P., Legras, B., Müller, R., and Riese, M.: Quantifying the effects of mixing and residual circulation on trends of stratospheric mean age of air, Geophys. Res. Lett., 42, 2047–2054, https://doi.org/10.1002/2014GL062927, 2015.

Prais, S. J. and Winsten, C. B.: Trend estimators and serial correlation, Cowles Commission discussion paper: Statistics no. 383, 1–26, 1954.

Prignon, M., Chabrillat, S., Friedrich, M., Smale, D., Strahan, S. E., Bernath, P. F., Chipperfield, M. P., Dhomse, S. S., Feng, W., Minganti, D., Servais, C., and Mahieu, E.: Stratospheric fluorine as a tracer of circulation changes: Comparison between infrared remote-sensing observations and simulations with five modern reanalyses, J. Geophys. Res., 126, e2021JD034995, https://doi.org/10.1029/2021JD034995, 2021.

Randel, W. J., Wu, F., and Stolarski, R. S.: Changes in column ozone correlated with the stratospheric EP flux, J. Meteorol. Soc. Japan, 80, 849 – 862, https://doi.org/10.2151/jmsj.80.849, 2002.

Rieder, H. E., Frossard, L., Ribatet, M., Staehelin, J., Maeder, J. A., Di Rocco, S., Davison, A. C., Peter, T., Weihs, P., and Holawe, F.: On the relationship between total ozone and atmospheric dynamics and chemistry at midlatitudes – Part 2: The effects of the El Niño/Southern Oscillation, volcanic eruptions and contributions of atmospheric dynamics and chemistry to long-term total ozone changes, Atmos. Chem. Phys., 13, 165–179, https://doi.org/10.5194/acp-13-165-2013, 2013.

Snow, M., Weber, M., Machol, J., Viereck, R., and Richard, E.: Comparison of Magnesium II core-to-wing ratio observations during solar minimum 23/24, J. Space Weather Space Clim., 4, A04, https://doi.org/10.1051/swsc/2014001, 2014.

Schoeberl, M. R., Douglass, A. R., Zhu, Z., and Pawson, S.: A comparison of the lower stratospheric age spectra derived from a general circulation model and two data assimilation systems, J. Geophys. Res., 108, 4113, https://doi.org/10.1029/2002JD002652, 2003.

Shangguan, M., Wang, W., and Jin, S.: Variability of temperature and ozone in the upper troposphere and lower stratosphere from multi-satellite observations and reanalysis data, Atmos. Chem. Phys., 19, 6659-6679, https://doi.org/10.5194/acp-19-6659-2019, 2019.

Shariff, N. A. M. and Duzan, H.: A Comparison of OLS and Ridge Regression Methods in the Presence of Multicollinearity Problem in the Data, International Journal of Engineering Technology, https://doi.org/10.14419/ijet.v7i4.30.21999, 2018.

Smith, A. and Matthes, K.: Decadal-scale periodicities in the stratosphere associated with the solar cycle and the QBO, J. Geophys. Res., 113, D05311, https://doi.org/10.1029/2007JD009051, 2008.

Sofieva, V. F., Tamminen, J., Kyrölä, E., Mielonen, T., Veefkind, P., Hassler, B., and Bodeker, G. E.: A novel tropopause-related climatology of ozone profiles, Atmos. Chem. Phys., 14, 283–299, https://doi.org/10.5194/acp-14-283-2014, 2014.

Sofieva, V. F., Kyrölä, E., Laine, M., Tamminen, J., Degenstein, D., Bourassa, A., Roth, C., Zawada, D., Weber, M., Rozanov, A., Rahpoe, N., Stiller, G., Laeng, A., von Clarmann, T., Walker, K. A., Sheese, P., Hubert, D., van Roozendael, M., Zehner, C., Damadeo, R., Zawodny, J., Kramarova, N., and Bhartia, P. K.: Merged SAGE II, Ozone_cci and OMPS ozone profile dataset and evaluation of ozone trends in the stratosphere, Atmos. Chem. Phys., 17, 12533–12552, https://doi.org/10.5194/acp-17-12533-2017, 2017.

Sofieva, V. F., Szelag, M., Tamminen, J., Arosio, C., Rozanov, A., Weber, M., Degenstein, D., Bourassa, A., Zawada, D., Kiefer, M., Laeng, A., Walker, K. A., Sheese, P., Hubert, D., van Roozendael, M., Retscher, C., Damadeo, R., and Lumpe, J. D.: Updated merged SAGE - CCI- OMPS+ dataset for evaluation of ozone trends in the stratosphere, Atmos. Meas. Tech. Discuss. [preprint], https://doi.org/10.5194/amt-2022-313, in review, 2022.

Solomon, P., Barrett, J., Mooney, T., Connor, B., Parrish, A., and Siskind, D. E.: Rise and decline of active chlorine in the stratosphere, Geophys. Res. Lett., 33, L18807, https://doi.org/10.1029/2006GL027029, 2006.

Steinbrecht, W., Köhler, U., Claude, H., Weber, M., Burrows, J. P., and van der A, R. J.: Very high ozone columns at northern mid-latitudes in 2010, 38,https://doi.org/10.1029/2010GL046634, 2011.

Steinbrecht, W., Froidevaux, L., Fuller, R., Wang, R., Anderson, J., Roth, C., Bourassa, A., Degenstein, D., Damadeo, R., Zawodny, J., Frith, S., McPeters, R., Bhartia, P., Wild, J., Long, C., Davis, S., Rosenlof, K., Sofieva, V., Walker, K., Rahpoe, N., Rozanov, A., Weber, M., Laeng, A., von Clarmann, T., Stiller, G., Kramarova, N., Godin-Beekmann, S., Leblanc, T., Querel, R., Swart, D., Boyd, I., Hocke, K., Kämpfer, N., MaillardBarras, E., Moreira, L., Nedoluha, G., Vigouroux, C., Blumenstock, T., Schneider, M., García, O., Jones, N., Mahieu, E., Smale, D., Kotkamp, M., Robinson, J., Petropavlovskikh, I., Harris, N., Hassler, B., Hubert, D., and Tummon, F.: An update on ozone profile trends for the period 2000 to 2016, Atmos. Chem. Phys., 17, 10675–10690, https://doi.org/10.5194/acp-17-10675-2017, 2017.

Stiller, G. P., Fierli, F., Ploeger, F., Cagnazzo, C., Funke, B., Haenel, F. J., Reddmann, T., Riese, M., and von Clarmann, T.: Shift of subtropical transport barriers explains observed hemispheric asymmetry of decadal trends of age of air, Atmos. Chem. Phys., 17, 11177–11192, https://doi.org/10.5194/acp-17-11177-2017, 2017.

Sukhodolov, T., Rozanov, E., Ball, W., Bais, A., Tourpali, K., Shapiro, A., Telford, P., Smyshlyaev, S., Fomin, B., Sander, R., Bossay, S., Bekki, S., Marchand, M., Chipperfield, M., Dhomse, S., Haigh, J., Peter, T., and Schmutz, W.: Evaluation of simulated photolysis rates and their response to solar irradiance variability, J. Geophys. Res.-Atmos., 121, 6066–6084, https://doi.org/10.1002/2015JD024277, 2016.

Soukharev, B. E. and Hood, L. L.: Solar cycle variation of stratospheric ozone: Multiple regression analysis of long-term satellite data sets and comparisons with models, 111, https://doi.org/10.1029/2006JD007107, 2006.

Szeląg, M. E., Sofieva, V. F., Degenstein, D., Roth, C., Davis, S., and Froidevaux, L.: Seasonal stratospheric ozone trends over 2000–2018 derived from several merged data sets, Atmos. Chem. Phys., 20, 7035–7047, https://doi.org/10.5194/acp-20-7035-2020, 2020.

Tirink, C., Abaci, S., and Önder, H.: Comparison of Ridge Regression and Least Squares Methods in the Presence of Multicollinearity for Body Measurements in Saanen Kids, Journal of the Institute of Science and Technology, 10, 1429-1437, https://doi.org/10.21597/jist.671662, 2020.

Tung, K. and Yang, H.: Global QBO in circulation and ozone. Part I: Reexamination of observational evidence, J. Atmos. Sci., 51, 2699–2707, https://doi.org/10.1175/1520- 0469(1994)0512.0.CO;2, 1994.

Wang, W., Hong, J., Shangguan, M., Wang, H., Jiang, W., and Zhao, S.: Zonally asymmetric influences of the quasi-biennial oscillation on stratospheric ozone, Atmos. Chem. Phys., 22, 13695–13711, https://doi.org/10.5194/acp-22-13695-2022, 2022.

Wargan, K., Orbe, C., Pawson, S., Ziemke, J. R., Oman, L. D., Olsen, M. A., Coy, L., and Emma Knowland, K.: Recent decline in extratropical lower stratospheric ozone attributed to circulation changes, Geophys. Res. Lett., 45, 5166–5176, https://doi.org/10.1029/2018GL077406, 2018.

Weber, M., Dhomse, S., Wittrock, F., Richter, A., Sinnhuber, B. M., and Burrows, J. P.: Dynamical control of NH and SH winter/spring total ozone from GOME observations in 1995-2002, Geophysical Research Letters, 30, https://doi.org/10.1029/2002gl016799, 2003.

Weber, M., Coldewey-Egbers, M., Fioletov, V. E., Frith, S. M., Wild, J. D., Burrows, J. P., Long, C. S., and Loyola, D.: Total ozone trends from 1979 to 2016 derived from five merged observational datasets – the emergence into ozone recovery, Atmos. Chem. Phys., 18, 2097–2117, https://doi.org/10.5194/acp-18-2097-2018, 2018.

Weber, M., Arosio, C., Coldewey-Egbers, M., Fioletov, V. E., Frith, S. M., Wild, J. D., Tourpali, K., Burrows, J. P., and Loyola, D.: Global total ozone recovery trends attributed to ozone-depleting substance (ODS) changes derived from five merged ozone datasets, Atmos. Chem. Phys., 22, 6843–6859, https://doi.org/10.5194/acp-22-6843-2022, 2022.

WMO: Scientific Assessment of Ozone Depletion: 2018, Global Ozone Research and Monitoring Project Report, World Meteorological Organization, Geneva, Switzerland, 588 pp., 2018.

WMO: Scientific Assessment of Ozone Depletion: 2022, GAW Report No. 278, ISBN 978-9914-733-97-6, 2022.

Xie, F., Zhang, J., Li, X., Li, J., Wang, T., and Xu, M.: Independent and joint influences of eastern Pacific El Niño–southern oscillation and quasi biennial oscillation on Northern Hemispheric stratospheric ozone, Int. J. Climatol., 12, 5289–5307, https://doi.org/10.1002/joc.6519, 2020.

Zhang, J., Zhang, C., Zhang, K., Xu, M., Duan, J., Chipperfield, M. P., Feng, W., Zhao, S., and Xie, F.: The role of chemical processes in the quasi-biennial oscillation (QBO) signal in stratospheric ozone, Atmos. Environ., 244, 117906, https://doi.org/10.1016/j.atmosenv.2020.117906, 2021.

Ziemke, J.R., S. Chandra, L.D. Oman, and P.K. Bhartia, A new ENSO index derived from satellite measurements of column ozone, Atmos. Chem. Phys., 10, 3711–3721, https://doi.org/10.5194/acp-10-3711-2010, 2010.